A ROBOPHYSICS APPROACH TO BIPEDAL WALKING IN GRANULAR MEDIA

A Thesis
Presented to
The Academic Faculty

by

Mark Kingsbury

In Partial Fulfillment
of the Requirements for the Degree
Doctor of Philosophy in the
School of Physics

Georgia Institute of Technology

August 2016

A ROBOPHYSICS APPROACH TO BIPEDAL WALKING IN GRANULAR MEDIA

Approved by:

Professor Daniel I. Goldman, Advisor
School of Physics
Georgia Institute of Technology

Professor Michael Schatz
School of Physics
Georgia Institute of Technology

Professor Kurt Wiesenfeld
School of Physics
Georgia Institute of Technology

Professor Patricio Vela
School of Electrical and Computer Engineering
Georgia Institute of Technology

Professor Jennifer Curtis
School of Physics
Georgia Institute of Technology

Date Approved: 6 May 2016

ACKNOWLEDGEMENTS

I would like to thank everyone that has supported, encouraged, and aided me during my tenure as a graduate student pursuing a PhD in physics. These people were invaluable to my advancement within my program.

First I would like to thank my PhD advisor, Prof. Daniel Goldman, for his support and mentorship in my research throughout the program. He provided valuable insight for regions of research to explore and encouraged me to follow my own ideas for further discovery and the means and equipment for me to do so. He helped develop and shape me as a researcher, instilling the necessary skills for research and presentation through weekly lab meetings in particular. I was allowed to travel to international conferences to present my research and learn from the larger field. My responsibilities within the lab such as mentoring undergraduate students and managing the machine shop further developed me professionally.

Apart from my advisor, I would like to thank my committee members: Prof. Kurt Wiesenfeld, Prof. Jennifer Curtis, Prof. Michael Schatz, and Prof. Patricio Vela for serving as members and for their encouragement.

I would like to thank Prof. Stephen Gatesy and Peter Falkingham for their involvement in earlier sections of my research and support during my early graduate career. Their work on the locomotion of guinea fowl built the morphology of the robot and provided valuable insight into different movement strategies. I additionally thank Prof. Paul Umbanhowar for conversations, insight, and support that he provided during early stages of my research.

I would like to thank my colleagues within and associated with the lab. Firstly I would like to thank Tingnan Zhang for his invaluable work providing the code

for simulating the robot within the Chrono::Engine. I also thank Miguel Serrano providing the base algorithm for generating gaits for the robot. Additionally I thank Vlad Levenfeld for his work on bipedal walking as I entered the lab and for creating the program that translated angular positions into serial commands to send to the robot. I am grateful for additional help from Dr. Christian Hubicki and Michael Grey for their work under Prof. Aaron Ames in applying insights gained from the robophysical biped to the humanoid HUBO robot. Beyond that, I must thank all the other members of the lab who have provided insightful comments during lab meetings or whose expertise has aided me in a particular area. Additionally I thank them for all their support and making my experience as a graduate student enjoyable for the past years.

I would also like to thank my undergraduate advisor Prof. Tom Solomon for his support and cultivation of my passion for research and for providing me with the opportunity to come to study at Georgia Tech.

I would like to thank my friends for their support and encouragement over the years. They have been there for me to help me through difficult times and provided a steady source of happiness and stress relief without my graduate career would not have been possible.

I must thank my family for their love and constant support. I am grateful for my parents, James and Sylvia Kingsbury, for encouraging and supporting me at every step. Additionally I thank my brothers, Eric and Allen Kingsbury, my sister-in-law, Jess Kingsbury, and my nephew, Jacob Kingsbury, for their continued support. I also thank my very patient fiance, Sara Alfano, for her strength and encouragement throughout my graduate career.

Lastly, I would like to thank my funding agencies for their financial support.

TABLE OF CONTENTS

LIST OF FIGURES

SUMMARY

Humanoid robots will need capabilities to traverse environments ranging from factory floors to disaster areas. However, most of today's devices fail when faced with more complex ground conditions such as loose sand and mud. Terrains comprised of granular media remains challenging as they can display solid and fluid-like features. These substrates provide solid-like constraint forces until the stress on the material exceeds the yield criterion and the material flows as a resistive fluid.

To uncover the principles of bipedal walking in these complex environments and improve techniques for robotic locomotion, we took a "robophysics" approach. Robots are used in experiment to uncover the physics guiding a form of locomotion in a particular environment. Insights gained from these experiments lead to improvements in real robots. The improved devices are used to further explore the physics of these environments.

First we studied the locomotion of an automated, planarized bipedal walking robot in dry granular media. We additionally modeled this robot using the Chrono::Engine, a multi-body simulator, with empirical Resistive Force Theory. Resistive Force Theory is a force model developed for fluids that describes forces in granular media to model the ground reaction forces.

These studies revealed that the differential slip that took place during the two-foot interaction. This is when the two feet moved relative to and pushed against each other in the granular media, one foot remained fixed in the material the other foot yielded through the substrate. This phenomenon originated from the fluid-like and solid-like properties of granular media. The material acted as a solid for the fixed

foot and a fluid for the yielding foot. We built on the Chrono::Engine simulation and explored self-balanced walking in granular media. In this material, the robot became unstable when the external torque exceeded the yield criterion of the substrate.

We applied the findings from the robophysical process and tested these results on a human scale humanoid robot, HUBO. While traditional strategies for walking on hard ground failed in loose material, the HUBO robot walked successfully in granular media under open-loop control.

We discovered that differential slip occurred during the two-foot interaction in granular media. The solid and fluid-like properties that caused this differential slip also caused walking to become unstable during the two-foot interaction.

CHAPTER I

INTRODUCTION

1.1 Motivation and overview

Robots move in complex environments to conduct search and rescue procedures [1], planetary exploration [2], and remote manipulation of the environment such as digging [3]. During the nuclear disaster in Fukushima, Japan in 2011, it became clear it was a challenge for robots to move within complex environments. When the environment was too dangerous for humans to enter and safely disable the reactor, robots of the time were unable to resolve the crisis due to the loose debris and unstable environment. With a robust means of entering and navigating areas too dangerous for humans, robots will significantly reduce the impact of natural and man-made disasters [4].

Animals have evolved different modes of locomotion such as walking, running, swimming, flying, jumping, and climbing. Robots have been able to replicate much of these locomotor modes to successfully navigate within the same sorts of environments. As shown in figure 1, robots run on hard ground [5], climb trees [6], swim in water [7], fly through the air [8], and walk bipedally over rough terrain [9]. However, loose terrain such as sand and mud provides a unique set of challenges for these locomotors [10]. The material exhibited fluid-like properties by yielding and flowing around an intruding segment according to the yield stress supported [11]. When the stress from a segment of the intruder is below this yield stress, the ground displayed solid-like properties with constraint forces. This produces complex behavior and resulted in poor kinematic performance.

Part of the challenge robots faced in these loose environments is the lack of comprehensive force laws. Control algorithms used to balance and allow a robot to move optimally within an environment often require smooth force equations to describe the state of the robot. No such smooth, continuous equations exist for these types of terrain, however. Often the only option to characterize ground reaction forces rely

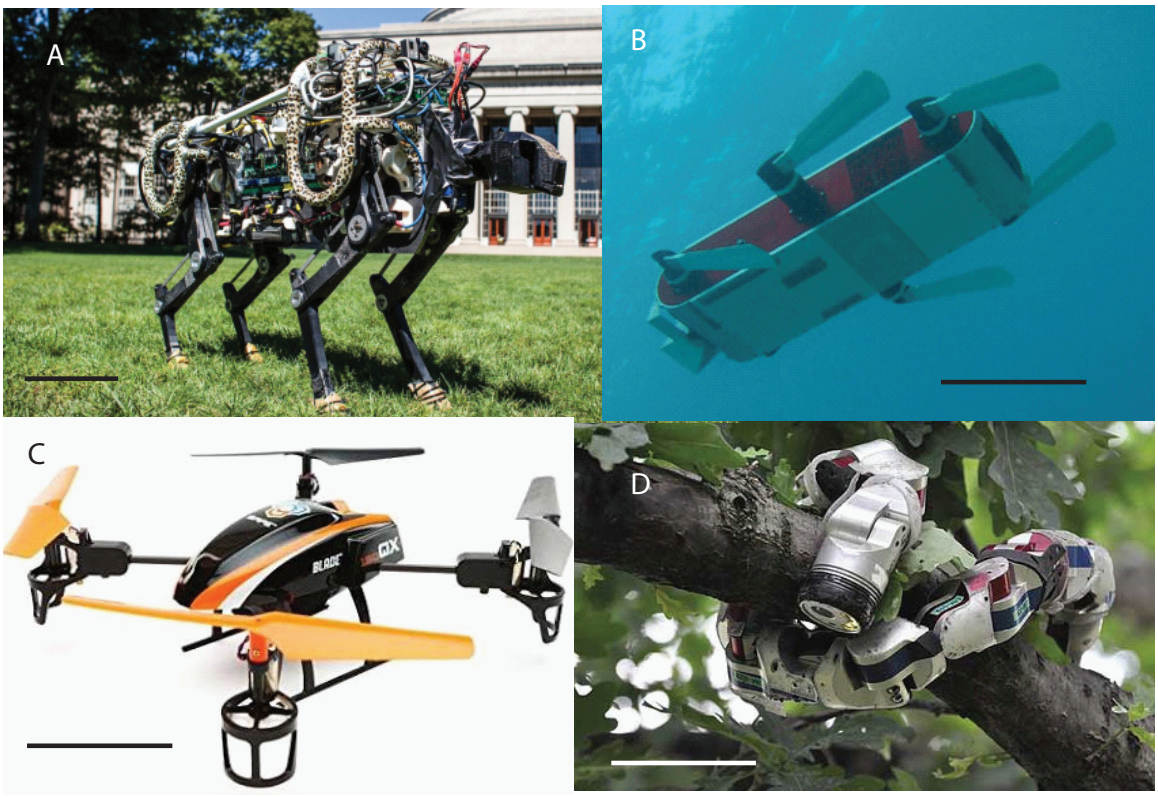

Figure 1: Robots used to move in different environments. Scale bars are 10 cm for each image. (A) Cheetah-inspired robot that ran across hard ground [5]. (B) R-Hex robot that swam through water [7]. (C) 180 QX quadcopter that flew through the air. (D) Snake-inspired robot that climbed trees [8].

on empirical force models that are not described by continuous equations. Without a strategy to address these loose environments, forms of locomotion such as walking that depend on these controllers for balance were particularly challenging.

This dissertation takes a robophysics [12] approach to study long-legged locomotion within these flowable substrates and develop general principles that guide this behavior. This methodology uses the systematic study and control of a simplistic robotic device to investigate the physics underlying this complex locomotion. In addition, this dissertation studies bipedal walking through the lens of Resistive Force Theory [13] to understand the effects of foot intrusion kinematics, the two-foot interaction, and material properties on this form of locomotion. This study not only advances our understanding of bipedal walking in complex terrains but reveals the importance of differential slip that is unique to interactions with flowable substrates. These results were applied to a human scale, humanoid robot, HUBO [14], to walk successfully in granular media. In the following sections of this chapter, we explore the foundation of this dissertation by examining previous work, different experimental techniques and theoretical bases.

1.2 Robophysics

In the emerging discipline of robophysics [12], instead of designing robots to accomplish a specific task or optimally fulfill a desired function, the robot is instead used as a tool with which to measure and discover physical principles. In robophysics, failures such as a robot failing to move effectively can be just as or even more valuable than successes. The robot is ultimately used as a physical model to study and explore the fundamental principles within a particular area. Robotic systems also allow for experimental automation to rapidly iterate through a parameter space.

This discipline stands at an intersection between robotics and physics. At the most basic level, a robophysical device is used to measure and explore physical behaviors. This survey of phenomena then improves physical models of the environment. These models are then applied to develop new strategies to improve robots. The process continues to iterate as robots are used to further test the newly developed model to

optimize performance. When experiment and model do not agree, we discover new regions of physics to explore and further improve the model. This additional testing provides the ongoing process that improves both our understanding of physics and performance in robotics with each step.

1.2.1 Automation in jumping on hard ground and granular media

One hallmark of a robophysics approach is its capacity for rapidly sweeping through a wide array of parameters (as shown in figure 2). An example of this aspect of robophysics is exemplified in an experiment on jumping on hard ground conducted with a simple hopping robot [15]. This simple hopping robot was a spring connected to a linear motor-driven rod that slid on a near-frictionless linear air-bearing. An automated, systematic experiment was conducted to study the physics of jumping with this 1-D hopper on hard ground. For each trial, a sinusoidal wave of differing frequency and phase offset drove the linear motor. The height reached of each jump was calculated by measuring the times of contact with a contact sensor between the ground and spring. The experiment was fully automated to cycle through parameters and store data without the need for human intervention, allowing for an exhaustive sweep of this parameter space with over 20,000 jumps captured. This mapping of the space identified different key modes of jumping such as the stutter jump and single jump. The automation protocol stood as the grounds for developing a model for this jumping behavior. The stutter jump mode achieved jump heights comparable to single jumps for a nearly an order of magnitude less power expended.

The jumping experiment expanded to jumping in prepared substrates of granular media [16]. While the stutter jump was an effective and efficient strategy for jumping on hard ground, it failed in granular media. Furthermore, different modes of jumping were sensitively dependent on the compaction of the material. The jump performance diminished in loosely packed states. Additional particle image velocimetry (PIV) of the granular media revealed that a cone of jammed granular media developed beneath the foot as it intruded into the material. This cone effectively changed the shape and mass of the foot during intrusion and required a novel set of equations

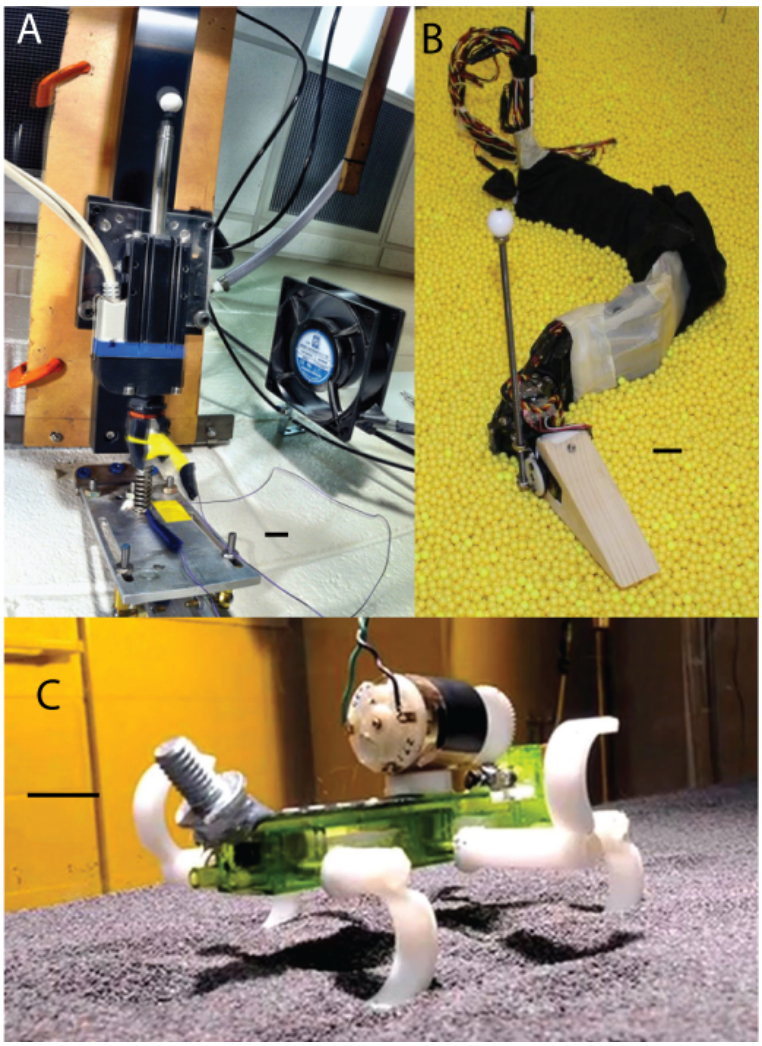

Figure 2: Simple robots used in a robophysics approach. Scale bar is 1 cm in each image. (A) Simple hopping robot used to study lift-off dynamics on hard ground [15]. (B) Sandfish-inspired robot used to study swimming in granular media [17]. (C) R-Hex style robot used to study legged locomotion in heterogeneous granular media [18].

to describe the interaction. Ongoing research optimizing the control of the jumping robot has additionally revealed areas where the current model does not agree with experiment, such as stopping and starting within the jump. This discrepancy between the experiment and the model has revealed new areas of physics in granular media to further explore.

1.2.2 Legged locomotion in heterogeneous granular media

The robophysics approach is demonstrated in a study of an R-Hex style XplorerBot moving in heterogeneous granular media [19], as shown in figure 2. Studies have examined the nature and locomotion principles within homogenoeous granular media, but little was understood about these forms of locomotion in heterogenous granular media. In nature, however, animals routinely contend with obstacles of sizes that differ by orders of magnitude such grains of sand and large boulders. This problem was complicated as there were not only interactions between the locomotor and the different material but also non-negligible interactions to be considered within the material itself. A struck boulder, for instance, slid in the material while it pushed against the limb segment.

To study moving in heterogeneous granular substrates, the XplorerBot was used in a fully automated experiment. Moving on a fluidized bed of poppy seeds, the robot automatically walked across the bed and interacted with a boulder. A gripper arm then recovered the robot and reset the experiment to automate the trials. To find the fundamental principles of this interaction, only a single boulder was used to measure the deflection and discover the effective potential of the boulder to the robot. This potential was sensitively dependent on where on the boulder the robot struck and with what limb the boulder was struck with. By using this empirical potential as a model for the interaction between robot and boulder, the robot was modeled in simulation moving over a field of boulders to measure the long term interaction with this complex environment.

1.2.3 Iterative modeling in subsurface sandswimming

Robophysics is an iterative process, as shown in a study of subsurface burial and swimming in granular media with the sandfish lizard used as a model organism [17]. This lizard readily and rapidly buried in a prepared substrate in laboratory settings. The sandfish swam by moving its body in an undulating wave beneath the surface. With x-ray video of the sandfish's subsurface behavior, a simple model of these oscillating, sinusoidal waves was created. A robotic device was designed from this model and used to conduct systematic experiments on the properties of the waveform in a granular media of plastic particles (figure 2). Animals are often not willing or not capable of changing movement parameters but a controlled robot allowed a full test of these variables. The effective dimensionless speed v, or body lengths per cycle, of the robot was measured by changing the relationship between amplitude A and wavelength λ. An optimal $\frac{A}{\lambda}$ was found that maximized v. These parameters agreed with the range of parameters and performance of the sandfish lizards.

The model for subsurface locomotion in granular media was revisited and improved after gaining insights with the robot. If the robot was a model for the animal, then a discrete element method (DEM) simulation was used to build a model of the model and further study this form of locomotion. The simulation tested the effect of head shape on swimming. This was then experimentally verified by attaching different shaped heads to the robot. In addition, a planar empirical resistive force theory was generated as force model [20]. The model divided the swimmer into segments of different cylinders moving within the material at different orientations and velocities. The forces on each segment were integrated over the body to get the entire force on the swimmer. With experimental and DEM simulation validation, it stood as a new model to understand granular swimming that was far less computationally intensive than the DEM simulations. Furthermore, the force model was valid only when the granular media acted as a frictional fluid without hysteresis. This provided insight that the sandfish lizard fluidized the grains around it while it swam in order to effectively move within its environment.

1.3 Granular media as model substrate for flowable terrain

A wide range of complex flowable substrates are found in nature. Animals and robots must contend with a range of loose terrain of varying properties such as sand, gravel, mud, leaf litter, and snow. These materials are challenging to maneuver through as the ground yields and flows around intruding segments, resulting in slip and becoming unbalanced. The range of materials that can be studied poses a challenge for conducting systematic tests on these environments. Even natural flowable terrain has drastic differences in constitution, particle size, angularity, cohesiveness, frictional properties, compaction, and so on. Performing exhaustive tests across the full range of substrates quickly becomes an unrealistic goal.

Dry granular media (GM) such as plastic particles and poppy seeds exhibits similar behavior to external forces as many of the materials listed above. However, these media have more regular shapes than natural sand (as shown in figure 3). These materials are therefore less computationally intensive to model individual grains in simulation. The state of these substrates are repeatedly controllable in experiment. The material is modeled in simulation as particles with repulsive and dissipative interactions. Thus dry granular media makes a simple, representative, and controllable model for flowable substrates.

1.3.1 Granular forces

Grain-to-grain interactions in granular media are described by normal and tangential forces [21]. The normal force is from the elastic deformation between the two grains in contact while the tangential force is from the friction between the contacting surfaces. Thus the individual grains interact with these repulsive and dissipative contact forces [22]. Furthermore, forces in granular media are carried by a small portion of the grains along spatially heterogeneous force chains [23]. These force chains then lead to complex dynamics of the bulk granular media.

When pressed by external forces, granular media remains in a solid-like state providing constraint forces until the external stress exceeds the yield stress of the material. Once this stress is exceeded, grains move and flow around the front of an

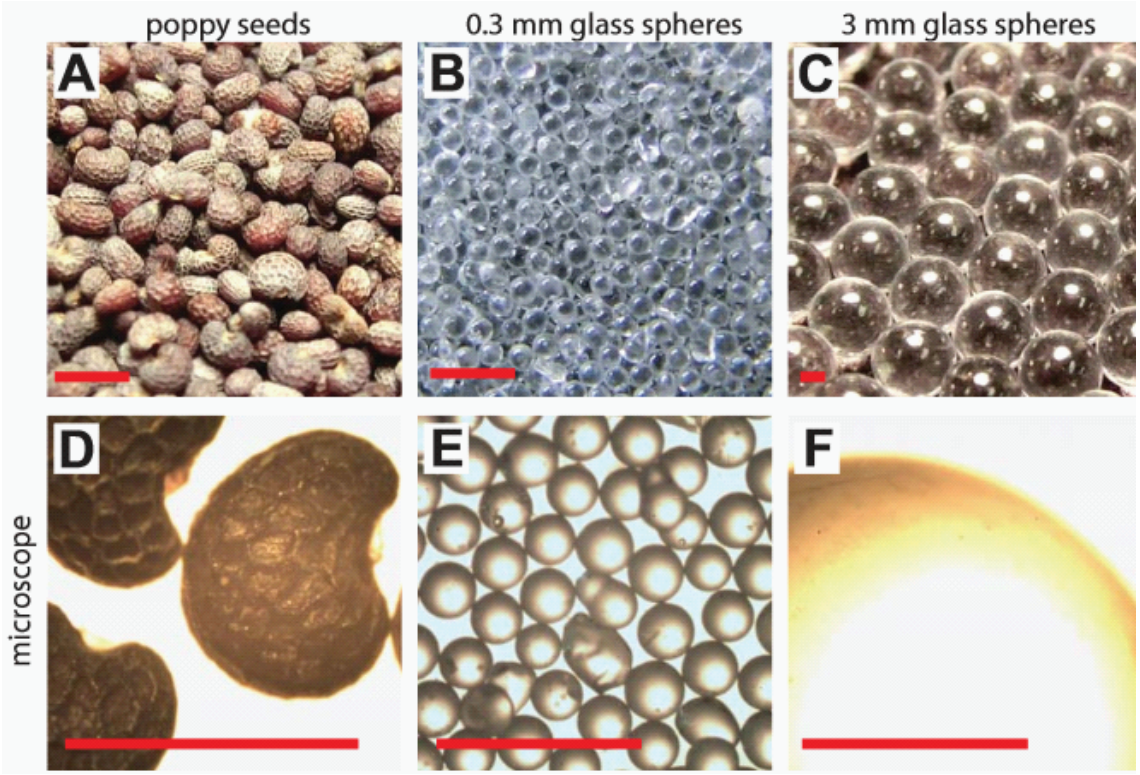

Figure 3: Different granular media viewed in bulk and under a miscroscope [13]. Scale bar is 1 mm in all images. (A) Poppy seeds. (B) 0.3 mm glass spheres. (C) 3 mm glass spheres. (D), (E), and (F) are respective microscopic views of these granular media.

intruder while the intruder experiences a resistive force from these grains. Regions of displaced grains are often locally isolated around the intruder. For slow speeds, this resistive force is independent of the velocity but scales with the depth and area of the intruder [24]. The velocity limit is bound by the speed that the grains are able to rearrange in front of the intruder. Above this speed, the inertia of the grains are non-negligible and the intrusion force scales quadratically with velocity. Previous studies have shown that the resultant resistive force was described as the sum of the velocity independent and dependent portions of the force [25, 26].

There is a frictional interaction in granular media perpendicular to the normal force and proportional to the normal force and the dimensionless inertial number of the material [27]. The inertial number I is described the the shear rate $\dot{\gamma}$, the particle diameter d, the normal stress P, and the particle density ρ_s as $I = \dot{\gamma}d/(P/\rho_s)^{0.5}$. The inertial number is interpreted as the ratio between the timescale of macroscopic deformation $(1/\dot{\gamma})$ and an inertial timescale $(d^2\rho_s/P)^{0.5}$. The experiments conducted here were dominated by the timescales for macroscopic deformation as the shear rate, $\dot{\gamma} = 0$ during static interaction between the foot and the grains. When the foot slipped through the grains, the shear rate reached as high as $\dot{\gamma} = 0.2$ s^{-1}.

1.3.2 Fluid and solid properties

Granular media exhibits solid-like and fluid-like behavior. Solids, when probed by an external force, provide constraint reaction forces. While there may be some elastic deformation, the solid provides forces equal and opposite to the external force. With fluids, however, an intruding object instead experiences a velocity-dependent resistive drag force. Granular media acts as a solid until the external force exceeds its yield stress in which the velocity independent (for $I < 10^{-3}$) resistive force will be applied to the intruder [27]. The material deforms around this object until the external force falls below the critical yield stress and the material resumes its solid-like properties. The yield stress is not only dependent on granular properties such as packing state and particle size but also on the parameters of the motion of the intruder within the material [28].

When external stresses are applied to the granular media, it is unknown whether and in what direction the material will yield. The Mohr-Coulomb model describes the three-dimensional stress distribution to evaluate whether there is a direction in which the yield criterion of the material is met [11]. The stresses applied to the material are characterized by the normal and tangential stress applied to a surface element. This surface element creates the Mohr circle as it rotates through the space when plotting the normal and tangential stresses. The material reaches the failure criterion when the stresses cross regions drawn by tangent lines on the circle and through the origin. The Mohr circle therefore provides not only the stress when failure occurs but also the direction in which this failure criterion is reached.

1.3.3 Volume fraction

The packing state of a granular media is described by the volume fraction ϕ. This is defined as the the volume of the grains divided by the volume of the occupied region. Thus the volume fraction is dependent on the arrangement of the individual grains. As granular media becomes more loosely packed, the volume fraction decreases. The volume of the grains remains the same across volume fractions. For homogenous, random packed granular media of roughly spherical shape, volume fraction ranges from $\phi \approx 0.57$ to $\phi \approx 0.64$ [29]. This range is also dependent on the coefficient of friction of the particles. Higher friction particles range to lower ϕ [30].

Different volume fractions have effects on the material properties of the grains. Higher ϕ exhibits higher yield stress and therefore more solid-like behavior [13]. In addition, there is a phase transition that occurs between loosely packed and closely packed GM around the critical packing state. This state occurs at a volume fraction of $\phi_C \approx 0.6$ [31]. When loose material is disturbed it contracts and become more compact, while compact material dilates and become looser. At the critical packing state, the material neither dilates nor contracts to in response to passing disturbances.

1.3.4 Preparation and control

To control the packing state of the granular media for experiments, a previous study used a fluidized bed that set volume fraction through air pulses [32]. The air-fluidized bed consisted of a granular media of poppy seeds that sat atop a rigid, porous material [33]. Several air inlets fed into a distributor beneath the porous material and pushed air up through the porous surface and the grains. When the air was forced at speeds such that the force of the air exceeded the weight of the grains, the media became fluidized. When the air flow rate was gently decreased, the media settled from this fluidized state into a uniform, loosely packed material with $\phi \approx 0.58$.

After this fluidization process, the air was pulsed for brief blasts exceeding the onset of fluidization. The grains packed with each pulse into denser states and reached volume fractions as high as $\phi \approx 0.63$ [32]. Another packing strategy used was to shake or vibrate the bed while the flow rate was held at just below the onset of fluidization. This method achieved similar ϕ depending on the length of time the grains were shaken.

1.4 Short-legged locomotion in loose substrates

There have been extensive studies in other forms of locomotion in granular media [32, 34, 35]. This loose terrain differed from hard ground in that it yielded around an intruder and acted as a frictional fluid when the forces from that intruder exceeded the yield stress of the material [32]. When the yield stress of the material exceeded the forces of the intruder, however, the material acted as a solid and provided effective constraint forces to the object. These materials also differed from fluids in that the ground-reaction forces were insensitive to the speed of the intruder for an inertial number I in the quasi-static regime [27, 32]). Furthermore, the environments exhibited hysteresis where they "recalled" previous disturbances and previously disturbed material exhibited different reaction forces [34].

1.4.1 Sensitivity to foot intrusion kinematics and volume fraction

Performance in loose substrates was sensitive to active limb kinematics. In a study of an R-Hex style robot, SandBot, the robot moved across a bed of poppy seeds at different volume fractions [32]. The hexapedal robot walked with c-shaped legs in an alternating tripod gait where each leg rotated through a cycle with fast and slow regions. The study shifted the onset of the slow region and the subtle kinematic change made the difference between whether the robot advanced during a cycle or failed to advance. This sensitivity was a result of the rotary walking of the SandBot and the material properties. In rotary walking, the material yielded about an intruding limb until it reached a depth that the ground stopped yielding and provided a static contact with the c-shaped leg. The robot then pivoted about the center of the curve of the leg to advance. When the leg moved quickly during this region, the material continued to yield and the robot failed to produce enough thrust to overcome its body drag.

This form of rotary walking was additionally sensitive to changes in volume fraction. As the yield stress of the material decreased with lower ϕ, the leg sank deeper in the material before the media solidified. The higher depth corresponded to a phase further in the leg's rotation, reducing the duty factor of the robot and decreasing its effective stride length. In loose material of $\phi = 0.58$, the substrate did not solidify during the leg's rotation and the robot failed to advance against its body drag regardless of limb kinematics.

1.4.2 Sensitivity to interacting with previously disturbed material

The hysteresis in granular media was observed during the locomotion of sea turtle hatchlings [34]. Mother sea turtles come ashore to lay a clutch of eggs in the sand on a beach. They use their flippers to intrude in the material and pull themselves along the sand while their body drags across the surface of the substrate. Upon hatching, the new sea turtles similarly use their flippers to pull themselves across the sand and down to the water. When moving on these granular surfaces, the sea turtles moved with a diagonal gait, alternately intruding a flipper into the material

and propelling themselves forward by lifting themselves and dragging their flipper back through the material. If the sea turtle's next step interacted with previously disturbed material from a prior cycle, however, the distance traveled within that cycle dropped significantly.

These locomotor principles were studied in depth using a biologically inspired robot (FlipperBot) [34]. The FlipperBot inserted plates into the granular media and then rotated these plates with respect to the body in a symmetric gait. After a few cycles with this gait, the FlipperBot's flippers began interacting with previously disturbed material. Once this occurred, the flippers no longer generated enough thrust compared to its body drag and failed to advance with each cycle. By analyzing videos taken of sea turtle hatchlings, it was observed that the hatchlings had a flexible wrist at the end of their flipper about which they pivoted. The same principle was implemented in the Flipperbot and allowed it to have the intruding plate rotate as a flexible wrist. The disturbed region within the granular media was significantly reduced by this change. Thus the robot maintained a level of thrust from inserting its flippers into the granular media to overcome its body drag and advance for multiple cycles.

1.4.3 Sensitivity to foot pressure and belly drag

Another consideration when studying movement in granular media was the effect of foot size and shape. While hard ground locomotion provided similar constraint forces as long as there was static contact, feet bearing the same mass but of smaller area penetrated deeper into granular media. A study examined the importance of foot morphology across multiple animals and robots [36]. These animals and robots moved across a fluidized bed of poppy seeds while their kinematic performance and leg penetration ratio were measured. The fluidized bed then pushed air through the granular media up to the onset of fluidization to measure the performance loss of each subject. This performance loss increased across robots and animals with greater foot pressure ($\frac{mg}{nA}$, where m is the mass, g is acceleration due to gravity, n is the number of limbs, and A is the area of a limb) as shown in figure 4. This corresponded

to the decrease in normalized speed as the leg penetration ratio increased. The feet of higher foot pressure experienced a greater leg penetration ratio as the substrate weakened. Two of the robots examined were the SandBot mentioned above and a smaller R-Hex style robot. When the ground fluidization reached a critical flow rate for these robots, the substrate no longer withstood the leg pressure and failed to support rotary walking. Again, each robot failed to provide significant thrust against their body drag. Animals that did not walk through rotary walking were less sensitive to changes in leg penetration ratio. Animals that walked with low leg penetration ratios never contended with belly drag and thus their kinematic performance was insensitive to changes in the ground state.

1.5 Long-legged locomotion on hard ground

1.5.1 Bipedal walking on hard ground

Bipedal locomotion on hard ground has been well studied in both animals and robots [37–39]. Bipedal walking animals such as humans stood as a physical model and benchmark for this form of locomotion [40] as well as inspiration for a robot's morphology [9]. These studies investigated not only locomotion on flat, level ground but also walking up and down inclines [41, 42] as well as walking over uneven (but still rigid) terrains [43]. Ongoing research is working to develop means of control to optimize this locomotion over these environments. These controls seek for robots to walk with stability [44] or to walk with minimal energy expenditure [45].

To describe bipedal walking, we divided this form of locomotion into two phases: The swing phase and the double-support phase. The swing phase is defined as the portion of the walking gait where one foot was out of contact with the ground while the other foot was planted. The double-support phase describes the regime where both feet were in contact with the surface. In its most basic form, a bipedal walker alternated between these two phases to move across hard ground.

In addition to different phases of walking there were also different types of walking. One form of walking was through quasi-static locomotion where intertial forces from the walker were negligible, or $F_{net} \approx ma$. This form of locomotion often took a single

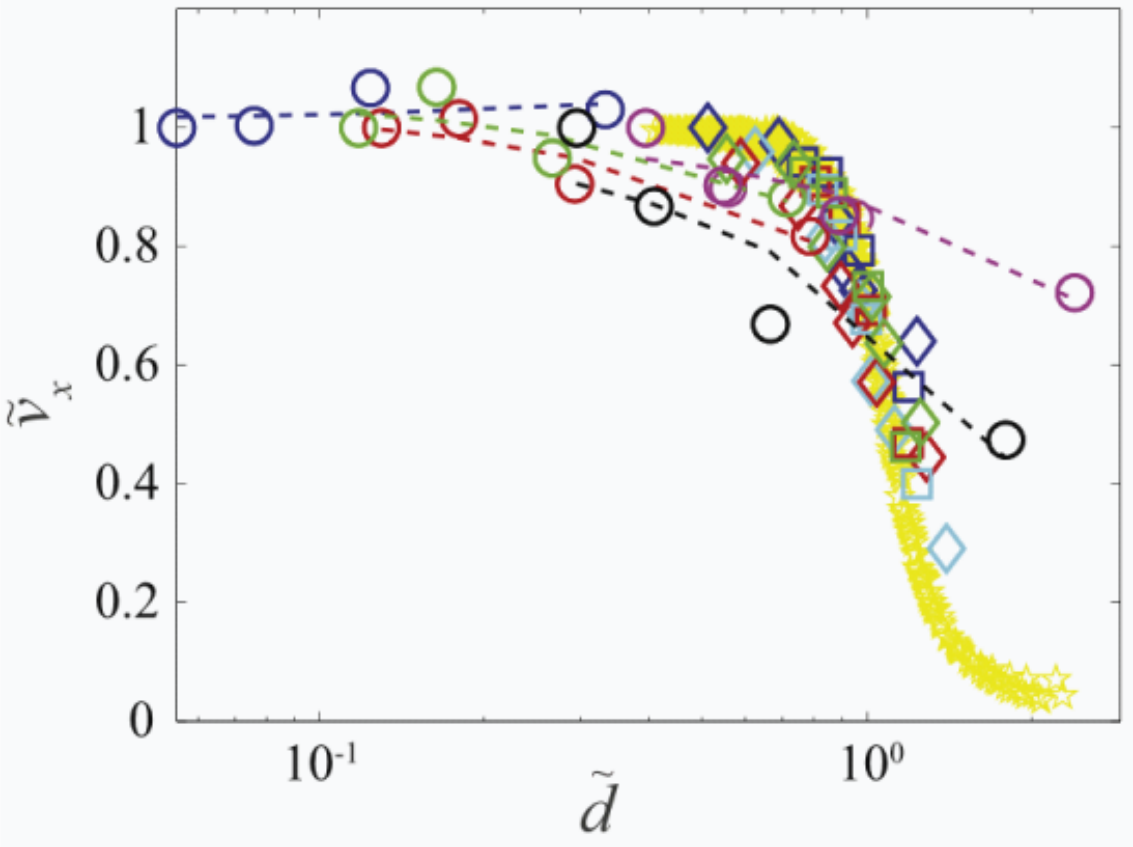

Figure 4: Normalized average speed vs leg penetration ratio for robots and animals [36]. Diamonds and squares are SandBot performance for different leg widths and colors corresponding to different gait frequencies. Circles of different colors match different animals moving in material at different flow rates. Yellow pentagrams are Xplorer in simulation using Resistive Force Theory. Dashed lines are trend lines for the different animals. Average speed decreased as leg penetration ratio increased. Animals were less sensitive to this relationship than the hexapedal robots.

step approach to walking. While some quasi-static walking robots walked successfully on hard ground [46, 47], the gait used was inefficient and did not match the walking performance of animals. A more natural looking form of bipedal was seen in dynamic walking. Dynamic walking models were not quasi-static and took the inertia of the robot into account. Instead the walker accelerated on push-off from the surface during the transition into the swing phase and decelerated during on impact with the ground during the transition back to the double support phase. Dynamic walking robots were often more efficient than their quasi-static walking counterparts [40] but faced additional complexities to model and control. We focused on quasi-static walking as a simple model for bipedal locomotion in this dissertation.

1.5.2 Maintaining balance

As shown in figure 5, a variety of robots of walked on hard ground. Walking models used for these robots used sophisticated control algorithms to allow for both stable and energetically efficient locomotion over hard ground [44]. These control systems allowed for responses to perturbations (such as kicking the robot) to correct for some unexpected torque and resume the previous walking gait after the event [48]. These controls additionally enabled a robot to walk across uneven terrain [49].

These control algorithms were built on the basic framework of inverted pendulum models [50]. In these models, the problem has been simplified to control the torque on an inverted pendulum to its contact with the ground. For quasi-static hard ground bipedal walking, as long as sufficient torque was provided by the actuator, stable walking was achieved as long as the projection of the center of mass of the walker was contained within the area of the foot. This center of mass was the equivalent of the center of pressure for this regime of walking, where the center of mass transitioned between the two stance feet during the double support phase and remained within the support polygon of the stance foot during the swing phase.

However, these advanced algorithms were only as robust as their model of the environment. For a bipedal robot model, these control schemes require sensory information to navigate the environment. A faulty model for this space often led to

catastrophic failure during bipedal walking and resulted in a fall. During the 2015 DARPA Robotics Challenge, many of the falls the robots experienced were from bad sensory information or a persistent external perturbation that was not accounted for in the model [4]. Moreover, some of these control schemes required smooth, integrable equations to describe the forces on the robot [44]. With loose terrain such as granular media, however, no such equations exist to describe the environment. Previous groups researched walking on loose or soft material such as urethane foam [51] or even granular media [52], but these studies relied on theoretical models with known problems in describing complex environments [13].

Even with complete knowledge of hard ground, the double-support phase was still of particular interest. When both feet were in contact with the ground, a two-foot interaction had to be considered. During this interaction, even slight differences in how the feet moved relative to each other resulted in slipping or providing additional torques to the locomotor that affected balance [55, 56]. Since these small discrepancies were difficult to control in robots and other models, many researchers condensed the double-support phase to a short duration to approximate this phase as an instantaneous interaction. The goal was to minimize the effects of any slipping or rotation [57, 58]. We identified this two-foot interaction that occured during bipedal walking in granular media and examined the role it played on kinematic performance.

1.6 Force models for ground reaction forces in granular media

While there have been many studies into legged locomotion in granular media, it was important to model ground reaction forces in these loose materials. These models provided valuable information on the instantaneous forces experienced by animals and robots. They additionally provided valuable insights on the fundamental principles on locomotion in these environments. We used the Resisitve Force Theory to model the robot used in experiment to gain insight into these principles.

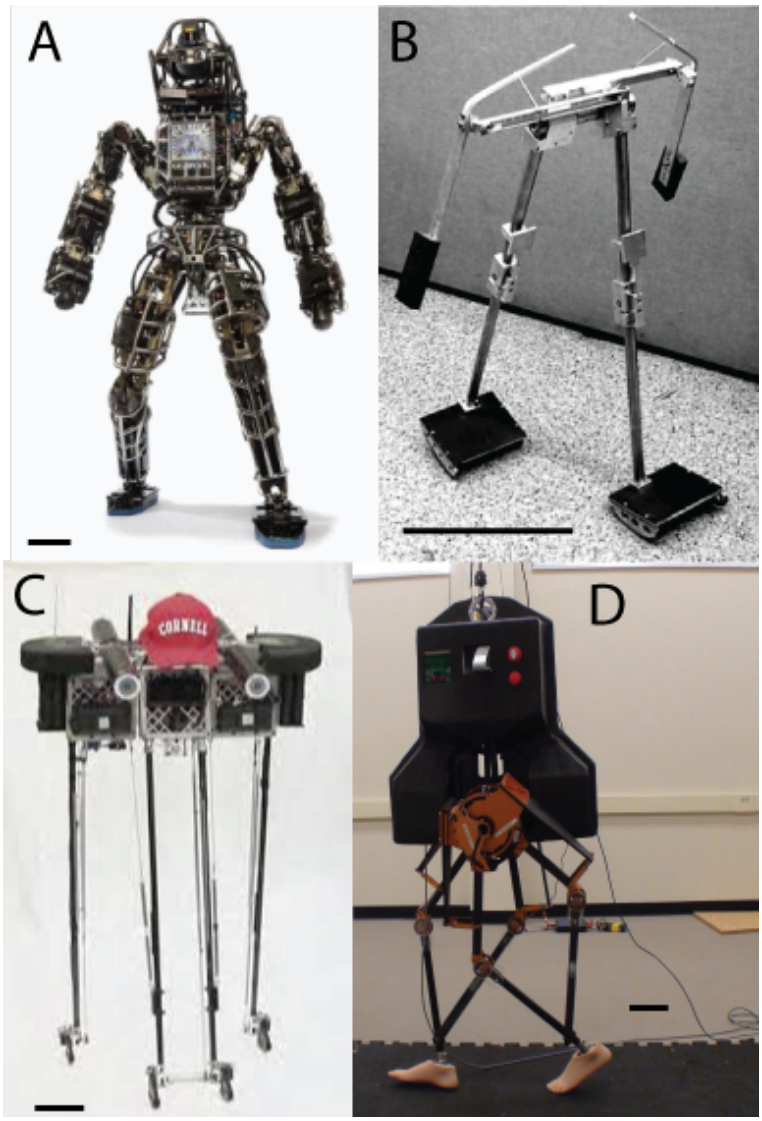

Figure 5: Bipedal robots that walk on hard ground. Bar is 10 cm in all images. (A) Atlas robot used by multiple groups in DARPA Robotics Challenge [4, 9]. (B) Passive dynamic walker that walks with human-like gait down slopes [53]. (C) Efficient bipedal walker built using passive dynamic principles [40]. (D) MARLO, an ATRIAS (Assume The Robot Is A Sphere) based robot that walks stably on hard ground [54].

1.6.1 Terramechanics

Terramechanics force models have been used to understand the force between wheeled and tracked vehicles and deformable ground since the 1950s [59]. These force models was derived from the systematic analysis of the normal load distribution of a vehicle's wheel or track and the soil or snow mechanics and deformation under that load. Utilizing pressure and sinkage relations, the shear stress and vehicle performance were accurately calculated for large wheeled and tracked vehicles. However, for smaller scaled wheels (wheel diameter less than 50 cm), prediction accuracy rapidly diminished due to the high curvature of the loading area which is missing from the flat-plate assumption built into the model [13]. This similarly proved a problem for legged locomotion as the flat-plate assumption did not hold over a variety of robot and animal legs and due to the complex interaction those legs had with the material.

1.6.2 Discrete element methods

To model the forces during locomotion in granular media, a multi-particle discrete element method (DEM) was coupled with a multi-body simulator software package (Working Model 2D) [20]. The DEM simulations modeled each individual grain for a volume of granular media and its interaction with some object or locomotor moving within it. The normal contact force was given by a Hertzian repulsion and a velocity dependent dissipation while the tangential contact force was modeled on Coulomb friction. Force parameters such as friction and dissipation were empirically tuned by matching simulated forces on intruders moving in granular media to experimental measurements. With the appropriate parameters, the DEM had accurate predictive power for a range of locomotion in different environments [13, 20].

Unfortunately, the DEM method is computationally expensive. Simulating individual grains becomes costly as more grains are simulated. Therefore DEM simulations are often reduced to simulating large particles with respect to the simulated area. Measuring long term dynamics becomes unfeasible given the length of the simulation and how long term dynamics additionally requires more particles to simulate a larger volume. Furthermore, this method proves impractical for rapid iteration for

sweeping through parameters.

1.6.3 Resistive Force Theory

To better understand this legged locomotion, a Resistive Force Theory (RFT) based empirical force model was developed [13]. Resisitive Force Theory was originally developed for fluid dynamics [60]. When an object was in a fluid flow, the force of the fluid acting on that object was understood by integrating the forces acting on each segment of that object. The forces on a small object of finite area were measured in experiment and used as the basis of the force acting on each segment. This model carried the assumption that the forces on each segment of an object correlated to the force on a test object from experiment. For fluids, this model had limited agreement with experiment [61, 62].

For granular media, empirical measurements were collected by inserting an acrylic plate of fixed area into granular media at different orientation angles and directions of motion with a 6 degree of freedom robot arm. A force sensor attached to the robot arm measured the ground reaction forces at each instantaneous depth. Ground reaction forces scaled linearly with the depth z and the area of the plate. Matrices of the vertical and horizontal ground reaction pressures were created for the plate orientation angle β and direction of motion γ. More complex intruders moving within the material were modeled by dividing the object into areas of different depth, orientation, and direction of motion and integrated over the area to determine the entire ground reaction force on the intruder. Thus the ground reaction forces on an object were understood as

$$F_{x,z} = \int |z| \alpha_{x,z}(\beta, \gamma) dA \tag{1}$$

where $\alpha_{x,z}$ is the scaled material response taken from experiment after accounting for area A and depth z. With different volume fractions and even different materials of varying particle size, shape, and density, the magnitude of $\alpha_{x,z}$ scales but the profile remains similar across this wide array of material parameters. Within these materials, a scaling law was found to connect the ground reaction forces. Only granular media with more disparate particle sizes and more angular shaped grains (such as natural

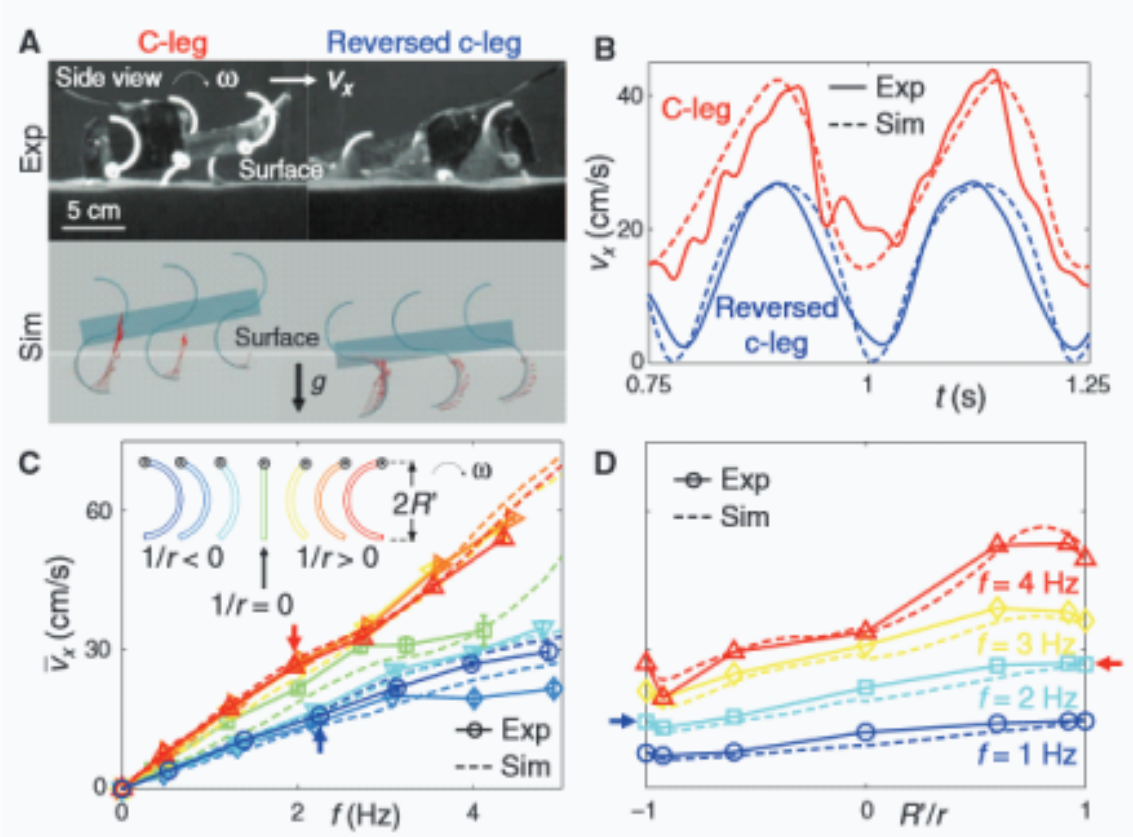

Figure 6: Agreement between RFT and experiment for XplorerBot [13]. (A) XplorerBot in experiment with C and reverse C shaped legs and robot modeled in simulation using RFT forces. (B) Comparison between simulation and experiment of x velocity vs time for C and reverse C shaped legs. (C) X velocity vs frequency across multiple foot shapes for simulation and experiment. (D) X velocity vs foot curvature across multiple frequencies for simulation and experiment.

sand) did not agree with this scaling.

RFT was implemented in a multi-body dynamics simulation (MBDyn) to test its agreement for the locomotion of a legged robot between experiment and DEM simulations. In these simulations, the robot was divided into segments of different instantaneous area A, orientation β, direction of motion γ, and depth z. The material was treated as a continuum which provided ground reaction forces on each segment depending on its individual parameters. By integrating over these forces, the robot moved within simulation. As opposed to previous studies using RFT for fluids [61], RFT in granular media demonstrated strong agreement for a variety of foot shapes

and kinematic parameters. An example for this agreement is shown with c-shaped legs in figure 6. Compared to DEM simulations, RFT simulations were far less computationally intensive and scale independent to particle size. Long term dynamics scaled linearly with time instead.

While RFT was generated as an empirical force law, Askari and Kamri discovered an underlying theoretical principle for these forces [63]. Modeling the granular media as a frictional-plastic continuum generated RFT and linked RFT to the behavior of the local material. While the local behavior of plastic material was complicated, dimensionless scaling for a segment that moved in this environment matched the superposition principle taken by RFT. Moreover, the scaling of RFT for a variety of materials was shown as the effect of parameters such as material density and gravity lumped into a single constant. In fluids, however, it was not possible to remove the factor of the length of the test segment from the forces measured. The local forces could not be separated from the chosen characteristic length.

We used the RFT examined here to simulate the robot and examine the instantaneous ground reaction forces it experienced during walking in granular media.

1.7 Organization of thesis

For the framework of this dissertation, Chapter II examines a bipedal walking robot and discusses the kinematic information across different parameters captured by that robot. Chapter III studies this robot simulated using the Resistive Force Theory and examines the kinematic and force information from those simulations. These findings were integrated with the experiment and simulation to uncover the principle of differential slip that occurred during bipedal walking. Chapter IV expands the simulation to allow for pitch and examines stability. These findings were applied to a human scale humanoid robot, HUBO, that walked successfully in granular media. Chapter V concludes the contribution of this dissertation and discusses research to be conducted in future work.

CHAPTER II

BIPEDAL WALKING ROBOT IN GRANULAR MEDIA

2.1 Summary

There have been few studies of bipedal walking in loose material such as sand and mud. These studies lacked a systematic approach to uncover the fundamental principles of this form of locomotion in these complex terrains. We used a robotic model for this locomotion and studied the effects of limb intrusion kinematics, foot size, and volume fraction ϕ of the material in a model substrate of poppy seeds.

To systematically sweep through these parameters, we created a fully automated experimental system to rapidly iterate through trials. A self-balancing robot requires additional degrees of freedom and a fundamental model of the substrate. As this robot was used to uncover these principles in walking, a linear air-bearing system planarized the robot and it walked with open-loop control. An Optitrack Camera system captured the intrusion kinematic information of the robot over varied volume fraction and foot area. Of these parameters, only foot size required human intervention to alter.

This study revealed a systematic asymmetry during the robot's walking gait from slight errors in the open-loop control accumulated across the motors. One foot's step would consistently experience more slip than the other. For both feet, there was a dependence on the limb intrusion kinematics for the amount of slip experienced by the robot. The robot was relatively insensitive to changes in volume fraction and foot size for the amount of slip experienced, although these changes were more significant under some limb intrusion kinematics.

2.2 Introduction

Bipedal walking has long stood as an area of research interest in the fields of robotics and biology. Researchers have sought to understand this locomotion and replicate

walking with robots to move through environments designed for humans. One application for these robotic systems was to enter in disaster areas too dangerous for humans [4]. However, when a location became cluttered with loose debris, walking in these environments was a challenge under current robotic systems. These challenges stemmed from the lack of comprehensive force models for these complex environment. As such there have been few studies examining bipedal walking within flowable terrain [52, 64].

Fortunately there have been many studies in multi-legged locomotion in loose material [32, 34, 35]. These systems had a natural stability that allowed for robust, open loop control in these complex terrains. With a simplified control system, the focus of the research instead fell on the fundamental physical interaction when maneuvering within these complex environments. Using a model substrate of granular media, these studies have revealed the importance that limb intrusion kinematics, volume fraction [32], and foot size [36] had for overall kinematic performance.

Using previous studies of multi-legged locomotion as a framework, we built a planarized bipedal robot to allow for open loop controls in loose ground. We used poppy seeds as a model substrate to investigate the fundamental principles of bipedal locomotion in flowable terrain. Building off previous techniques of experimental automation, this study examined the effects of foot-intrusion kinematics, volume fraction, and foot size on the performance of a bipedal walker and how that related to previous studies. We revealed that bipedal walking displayed a sensitivity to changes in foot-intrusion kinematics and the two-foot interaction but was robust to changes in both volume fraction and foot size.

2.3 Materials and methods

2.3.1 Volume fraction calibration

We conducted this experiment in a fluidized bed using poppy seeds as the granular media [32]. The bed comprised of 4 leaf blower motors to force air into a distributor beneath the bed and through a porous plastic material beneath the grains. Upon reaching the critical flow rate for the material, the poppy seeds fluidized and reset

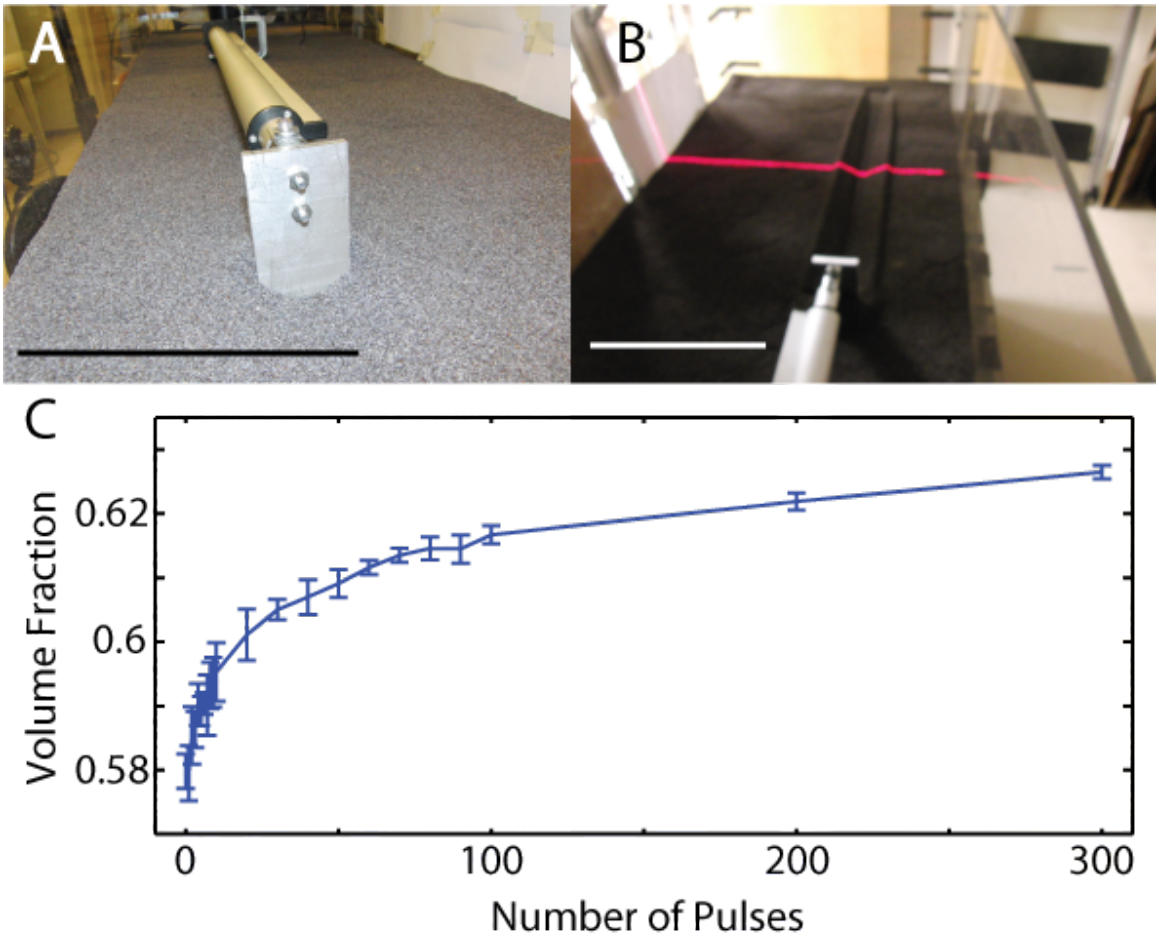

Figure 7: Calibration of volume fraction on fluidized bed. Scale bar is 10 cm in both images. (A) Linear motor dragging plate through prepared granular surface. (B) Laser line used to measure bed height and granular dilation/contraction to find critical packing state. (C) Relationship of number of pulses of air to achieved volume fraction.

the ground state to a uniform, loosely packed sate. In addition to resetting the material, the fluidized bed also controlled the volume fraction, ϕ, of the granular media. After initial fluidization, the air rapidly pulsed at flow rates past the onset of fluidization but at time scales before the bulk media entered a fully fluidized state. Under this protocol, with pulses for 0.1 s and time between pulses of 1 s, each pulse shook the grains into increasingly compact states.

An FA-400-L-12-24 Firgelli linear motor held suspended above the surface calibrated this compaction protocol. The linear motor arm dragged an attached metal plate through the material as it extended or retracted. A laser line suspended above the bed cut a line perpendicular to the path of the plate. A webcam set at an angle to this laser line captured an image of the position of the line [65]. We calibrated the height of the line with plates of known height from the pixel position in the webcam images. Each trial fluidized the granular bed followed by a controlled number of taps. The webcam captured an image of the surface of the granular media before and after the motor pulled the plate across the surface.

Given the spatial information on the change of height of the granular media from the plate's disturbance, the experiment measured whether the material was dilating, consolidating, or remaining the same from this disturbance and what change of volume was experienced. Compact material dilates upon disturbance, loose material consolidates, and a material in the critical packing state keeps constant volume. As the critical packing state of poppy seeds is known as $\phi \approx 0.6$ [31], this provided a calibration for the fluidizing and tapping protocol as shown in figure 7.

2.3.2 Planarized bipedal robot

To conduct repeatable experiments of bipedal walking on granular media, we created an eight motor bipedal robot (30.3 cm tall, 1.6 kg) as shown in figure 8. Each leg comprised of 4 HSR-5980SG digital servo motors from Hitec Robotics. An SSC-32 controller card from Lynxmotion controlled these motors. We connected the servo motors in series with aluminum brackets to mimic the general leg morphology of a guinea fowl, a bipedal bird whose locomotion has been investigated over loose and

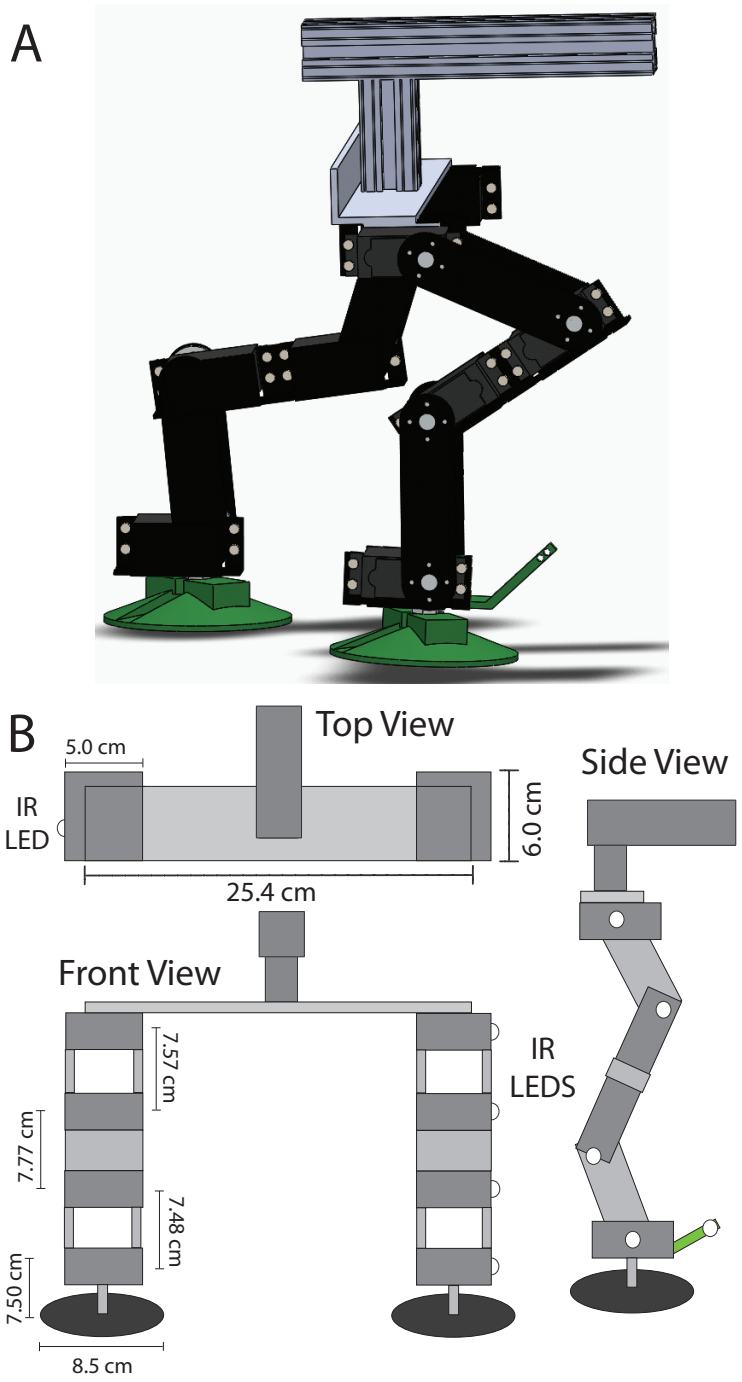

Figure 8: Design of bipedal robot. (A) Digital rendering of the bipedal robot used in the experiment. (B) 2D schematic representation of the robot from top, front, and side perspectives.

hard ground [66]. Attached to the bottom of each limb was a conical 3-D printed PLA plastic foot 8.5 cm in diameter. The bottom of each foot was coated with a layer of poppy seeds, the same material used to walk in. We conducted additional experiments with smooth plastic feet of the same diameter without the poppy seed coating as well smooth plastic feet of foot diameters ranging from 7.0 to 10.0 cm in diameter by increments of 0.5 cm.

2.3.3 Robot control scheme

The experiment controlled the robot in an open loop method. This position controller used angular positions for each motor calculated at 3 ms time intervals. The robot was over actuated for planar locomotion, requiring a robust means of generating angular positions for each motor to achieve the desired walking gait. Using a means developed by Miguel Serrano, a PhD student in Patricio Vela's group, we generated angular unique angular positions for each motor at each time step for a given gait. An additional executable converted these positions into serial commands and sent the commands the controller card. We found conversion between angular position and the serial commands for each motor by measuring the changes in angle against corresponding changes in serial position for each servomotor. The controller board processed these commands and fed them into the individual servo motors which moved to their desired positions by comparing against their internal potentiometer.

The base algorithm created by Miguel Serrano calculated the angular positions for each 3 ms time step in advance. This algorithm took as input the dimensions of the robot and starting angular position of each joint as well as specified positions for the tip of the toe and the center of the foot at each time step. Given the change in position and angular velocity of each joint in the limb for each time step, the code used a least-squared fitting method to minimize these parameters and determined the angles of each segment for the next time step.

With his method as the basis for calculating these trajectories, we saved this information out and repeated the process for the next step. This program only calculated the trajectory for one limb for a total of 12 steps, with the second limb

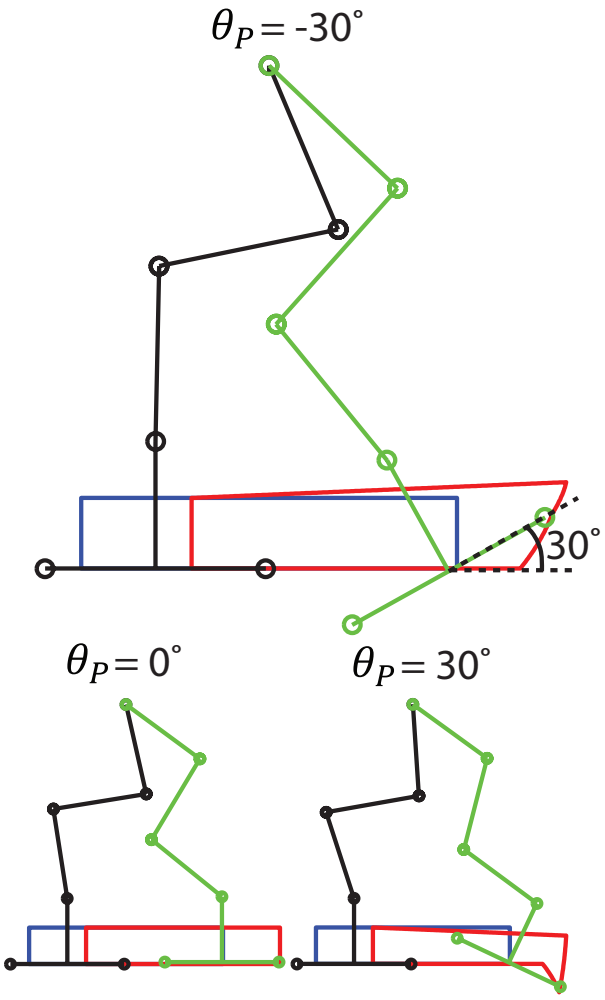

Figure 9: Walking gaits for the bipedal robot. (A) Depiction of the robot's $-30°$ presentation angle walking gait. The center of each foot was set to trace out the same blue rectangle for all presentation angles. The tip of the leading toe followed the red trajectory, where the presentation angle is defined as the maximum angle that the foot reaches upon intruding into the material. Command gaits for 0° (B) and 30° (C) presentation angles.

using the same angles phase shifted by π radians. After calculating the gait for walking 12 steps, the process was repeated using the ending angles of the first 12 steps as the starting position for the next 12 steps. This was done to minimize the impact of the starting position and have each step as uniform as possible.

We designed simple rectangular gaits to study the two foot interaction and the effects of foot intrusion kinematics during walking in granluar media (as shown in figure 9). The center of the foot always followed the same trajectory, tracing a

rectangle of 16 cm in width symmetric about the center of the robot and of 3 cm height which was sufficient to lift foot above the material during swing phase. The robot walked in a quasi-static regime with a total period of 6 seconds was defined with the foot spending $\frac{5}{8}$ of the period moving at uniform velocity with respect to the center of the robot on the bottom of the rectangle. This was to ensure that the robot was firmly in the walking regime with a definite period of two-foot interaction. The remaining portion of the gait consisted of lifting, lowering, and moving of the foot over the top line of the rectangle at uniform speed with respect to the center of the robot. While the motion of the center of the foot remained constant, the, the angle of the tip of the toe with respect to the center of the foot varied by what we defined as presentation angle, or the maximum angle the foot reached upon intruding fully into the material. We defined the front tip of the foot intruding into the material as positive presentation angle. This angle changed at constant angular velocity from its zero position at the moment of highest extrusion. Upon intruding fully into the material and reaching the full presentation angle, the foot uniformly returned to its level position before its other foot began lifting.

2.3.4 Automation protocol

We conducted repeated, controlled experiments, with the robot walking on an air-fluidizable bed of ∼1 mm diameter poppy seeds (50 cm wide, 250 cm long, ∼10 cm deep) [32]. After each experiment the bipedal robot automatically lifted off of the material using a linear motor while air pushed from underneath the bed through a porous material. The air flowed past the fluidization point causing the material to bubble. When the air flow turned off, the material settled into a uniform, loosely packed state of volume fraction, ϕ, 0.580 ± 0.005. Additionally, after the material settled, the air pulsed at the same intensity for 0.1 seconds and then turned off for 1.0 seconds. Each pulse made the material more compact and achieve a higher volume fraction (up to compact state of $\phi = 0.625 \pm 0.005$) as a function of the number of pulses. A webcam captured the image of the bed height of the granular media indirectly measured the volume fraction given the known relationship between

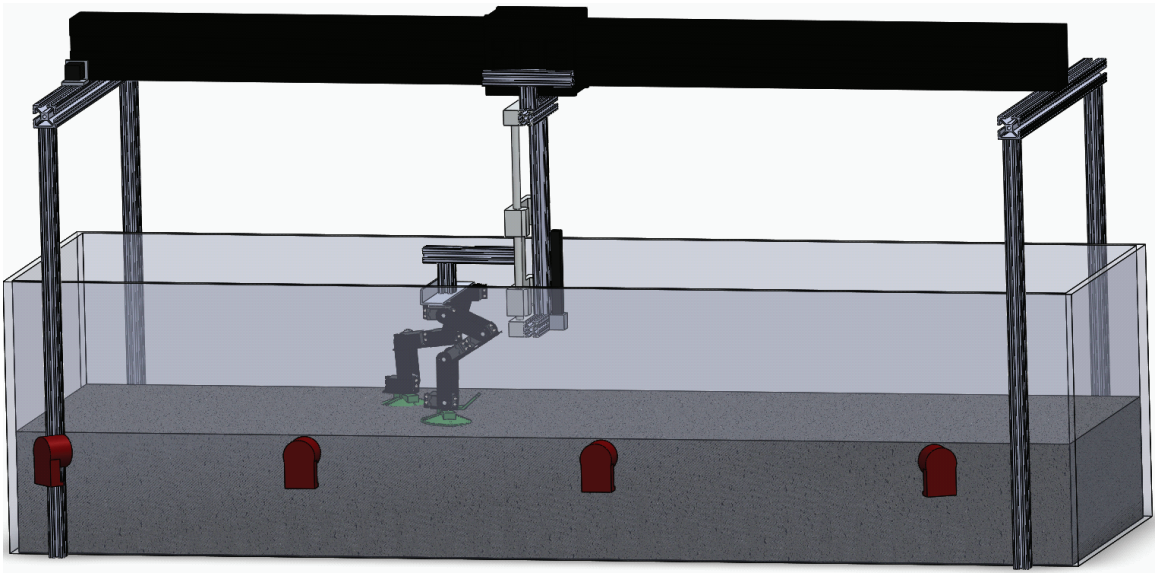

Figure 10: Experimental apparatus for automation of bipedal robot. This is a digital rendering of the robot connected to the full apparatus. The robot is planarized by the horizontal and linear air bearings to walk over the fluidized bed of poppy seeds. A linear actuator was connected along the vertical linear air bearing that was used to lift the robot from the granular media after each trial. A small, stepper motor was used to wind the robot back into the starting position after each experiment. The OptiTrack Red 13 3D cameras are shown staged in front of the apparatus.

height and compaction.

We attached the robot to two low-friction, linear air bearings connected orthogonal to each other. The horizontal air bearing ran along the span of the fluidized bed while the vertical air bearing was attached on the horizontal air bearing's carriage. The bipedal robot was fixed to the vertical air bearing's carriage. Thus the air bearings "planarized" the robot to move in the vertical and fore-aft directions but constrained it in all other directions. This planarization eliminated issues of balance that were beyond the scope of this study in walking in granular media. A stepper motor tethered to the horizontal carriage remained passive while the robot was walking but pulled the robot back to its start position after it was lifted from the material and a new ground state was being automatically prepared beneath it. A Magnetech Corp electoromagnet secured the carriage against a metal plate in the same initial position for each experiment as it was lowered and then released as it began its walking. A Hall-effect sensor at the end of the trackway automatically identified when the robot had finished an experiment to stop the run and lift the robot to begin again. Additionally, a contact sensor attached to the vertical air bearing connected if the robot failed to move in the material and no longer supported its own weight. The experimental trial then stopped at this point to lift the walker from the material and begin again.

We fixed IR LED's to the side of the robot at the connection of each limb segment with an additional LED added to rotate rigidly with the foot. 4 OptiTrack Red 13 3D cameras captured the 3D kinematic data of each IR LED marker to measure the limb's kinematics at 120 frames per second. Additionally a high resolution digital web cam recorded videos of each experiment at 60 frames per second. The full experimental apparatus is depicted in figure 10.

2.4 Measuring asymmetry

The physical robot exhibited a distinct asymmetry with each step: One foot consistently slipped further than the other leg. Using the web cam video, we corrected for distortion using the known segment length of each limb and measured the stride length and standing height of each limb. An individual servo motor erred in angular

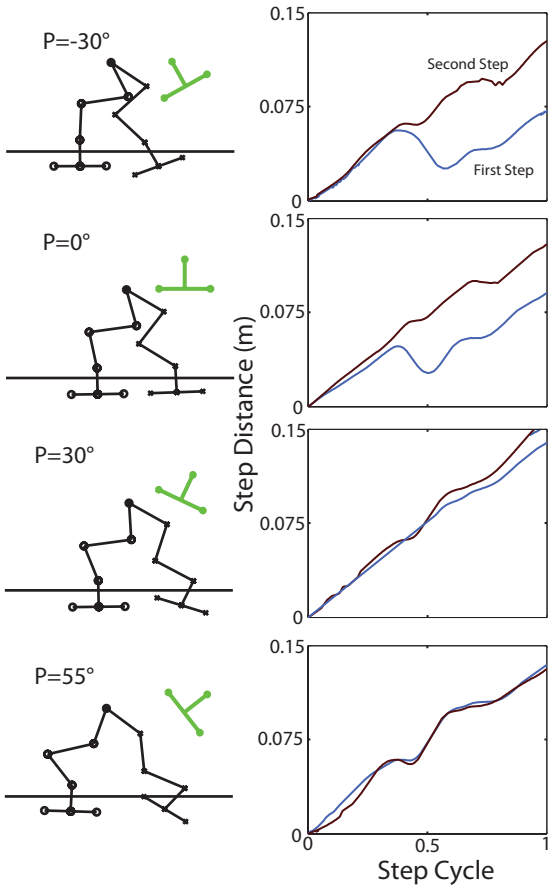

Figure 11: Walking performance on poppy seeds over different presentation angles. Shown are graphs of step distance vs step cycle for 4 different presentation angles for $\phi = 0.62$, 8.5 cm foot diameter with a coating of poppy seeds on the bottom. An asymmetry was found between each odd and even step although each experiences a region of slip during the onset of intrusion. Performance increases for steps of higher presentation angle.

position up to 5^o. This error accumulated across the 4 servo motors in each leg such that one foot consistently stepped less far than the other and one foot stood higher in the material than the other. These errors varied as a function of presentation angle.

2.5 Results and discussion

2.5.1 Sensitivity of foot-intrusion kinematics

As shown in figure 11, we observed a pronounced asymmetry between the two steps. For a particular volume fraction, the robot consistently had a lower step distance for

one the step from one foot than the other. This loss of step distance was consistent for which foot was performing more poorly across compaction and foot size although it varied with volume fraction. Therefore every odd step followed a particular kinematic profile while every even step would follow a different one within a trial.

This loss of step distance occurred during the onset of the two-foot interaction within the granular media, which is the intrusion phase. It manifested in a form of slip where the planted foot slid back (negative slip) or even forward (positive slip). Otherwise, no slip was observed during the swing and even the extrusion phases.

Gaits with more negative presentation angles invariably experienced more negative slip for both odd an even steps, although this slip was more pronounced in odd steps. The slip was minimized or even positive for more positive presentation angles up to 30^o but the slip increased for higher presentation angles. For presentation angles up to 55^o, the foot interacted and dragged across the granular media during the swing phase. The slip was therefore not from the typical intrusion phase but from the interaction experienced while dragging the foot at steep angles across the surface.

2.5.2 Dependence on volume fraction

Bipedal walking on granular media was insensitive to changes in volume fraction as depicted in 12. Despite this range of volume fractions accounting for up to a factor of two difference in ground reaction forces, the step distance of the robot was largely unchanged across presentation angles and the asymmetry.

We observed an exception to this insensitivity: The step distance dropped significantly with low volume fraction and high presentation angle. At these low volume fractions, the ground stiffness decreased and the robot stepped lower into the granular media. However, the orientation of the foot during the swing phase changed with different presentation angles. For larger presentation angles, the swing foot angled more towards the material. Therefore the swing phase reflected an additional period of two-foot interaction where the swing foot dragged across the granular media before the intrusion phase.

The overall insensitivity to ground state of the granular media differs significantly

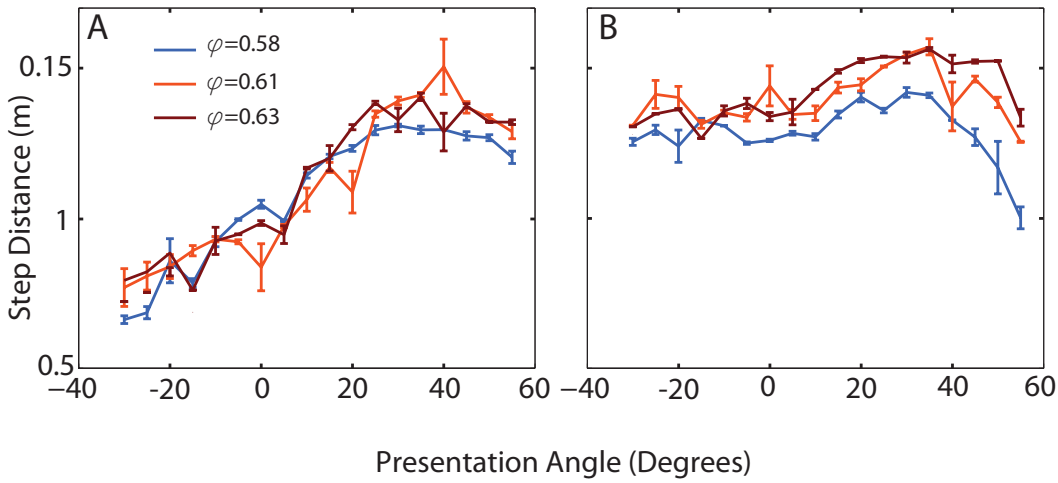

Figure 12: Walking performance on poppy seeds over different volume fractions. (A) Step distance vs presentation angle for the first step while (B) is the for the second step for 3 different volume fractions. Changes in performance are relatively insensitive to changing in volume fraction with a noted exception for high presentation angles. At lower volume fractions, the robot had higher leg penetration ratio and would experience a two-foot interaction during the swing phase as the highly angled foot would not remain clear of the material.

from a previous study on legged locomotion of SandBot in granular media [32]. However, the rotary walking used in this form of legged locomotion was characteristically different from bipedal walking. During rotary walking, the rotating foot intruded in the material until the resitive force matched the weight of the robot. The SandBot then rotated about the center of the curvature of its leg and advanced forward. Lower ϕ with lower ground reaction forces corresponded to the leg intruding deeper into the material before it solidified, reducing the effective stride length of the robot. At $\phi = 0.58$, the robot did not rotary walk and instead swam through the granular media as the material remained in the fluid-like regime to the legs. Bipedal walking had characteristically different phases of locomotion. Outside of the two-foot interaction, the stance foot remained in static contact with the granular media. As long as the swing foot stepped out of the material the walking robot was insensitive to changes in the magnitude of ground reaction forces.

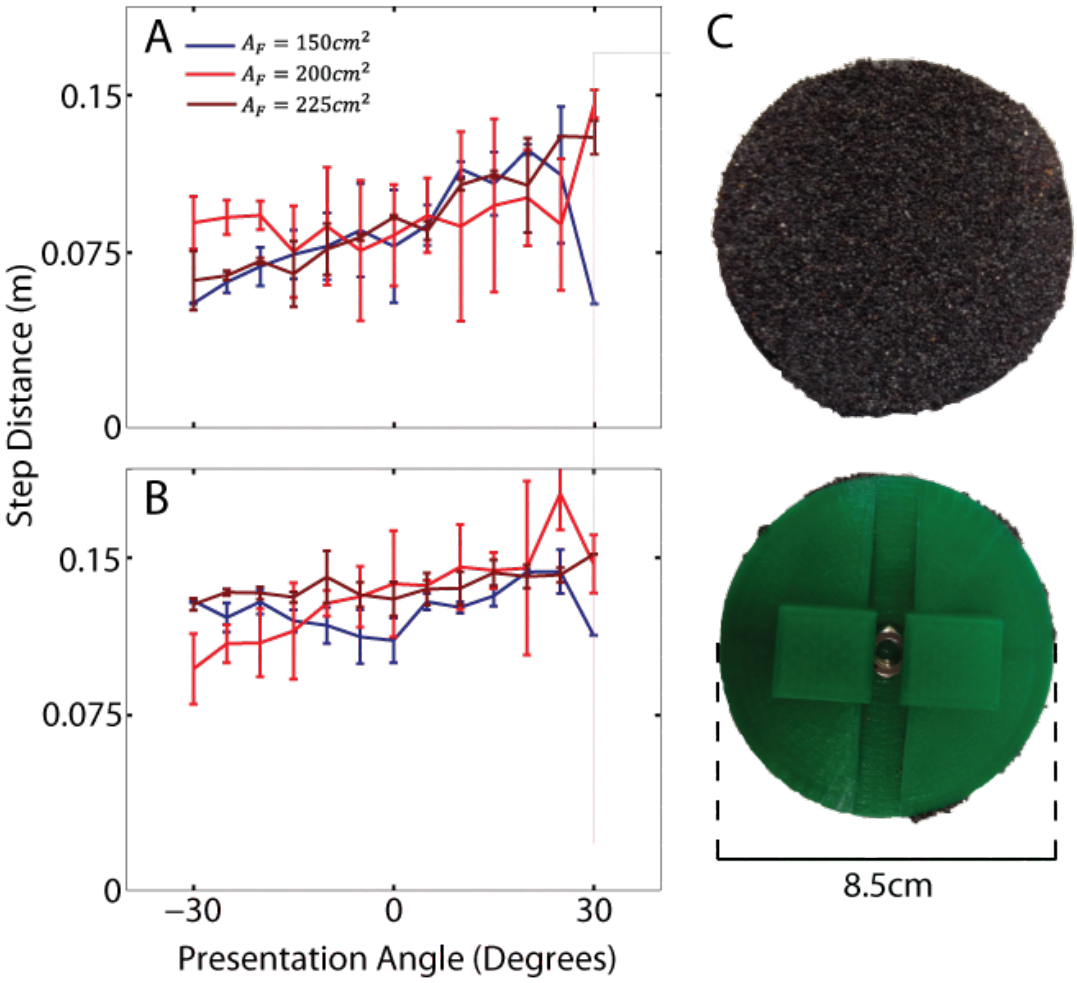

Figure 13: Effect of foot area on bipedal walking. (A) and (B) respective first and second step distance versus presentation angle for circular feet of different area for volume fraction $\phi = 0.61$. (C) Top and bottom of the 225 cm^2 which has additional poppy seed coating on the bottom of the foot (other feet have smooth plastic on bottom of feet).

2.5.3 Effects of foot area

Similar to the effects of changing volume fraction, figure 13 shows the step distance of the robot was insensitive to changes in foot area and frictional interaction between the surface of the bottom of the foot and the particles. This suggested that the kinematic performance of bipedal walking on these flowable substrates was largely independent of the direct frictional contact between the grains and the foot.

As we have seen from Qian et. al [36], changes in foot area corresponded to a proportional change in foot pressure. The robots in that study again walked with a form of rotary walking [32], providing a similar sensitivity to changes in foot pressure. However, organisms such as the zebra tailed lizard suffered minimal performance loss with changes in effective foot pressure. The animal was still capable of rapidly stepping in and over the material. Similarly, the step performance of the robot was insensitive to changes in foot area as the robot was still capable of stepping from the material and maintaining static contact with the stance foot.

2.6 Conclusion

While other forms of legged locomotion on granular media can be sensitive to foot size and volume fraction, the bipedal walking robot studied here was largely insensitive to these changes. Instead the most significant impact on step distance for this robot was the presentation angle, or foot intrusion kinematics with which it walked. By examining not only the magnitude of this loss in step distance but when during the cycle it took place, we identified that the two-foot interaction experienced during intrusion had the greatest impact of explored parameters on this walking behavior.

CHAPTER III

SIMULATING BIPEDAL WALKING IN GRANULAR MEDIA AND INTEGRATING WITH EXPERIMENT

3.1 Summary

To test models of legged locomotion in flowable substrates, other studies have used computer simulations to gain insight into the principles behind this locomotion. Results from simulation were then compared to experiment to test the accuracy of a physics model. Additionally, instantaneous forces on each segment found in simulation that were experimentally difficult to measure provided another tool to gain fundamental insight into locomotion in loose material.

This chapter detailed a simulation created by Tingnan Zhang of the bipedal walking robot using a Chrono::Engine with RFT based ground reaction forces. It examined results from this simulation and the effects of limb intrusion kinematics and volume fraction on bipedal walking in loose environments. As with the experiment, the slip experienced occurred during the two-foot interaction in the intrusion phase. In addition, the foot forces over the entire foot were simulated for different movement parameters. Resistive forces for the whole foot provided more intuitive understanding on the forces experienced by the robot. We then examined results in experiment through the lens of the simulation to understand the differential slip that occurred during the two-foot interaction in granular media.

3.2 Introduction

Previous studies for understanding the fundamental principles of locomotion in complex terrain included computer simulation models [20]. These simulations allowed for rapid iteration on different movement strategies, provided instantaneous forces acting on different segments of an intruder, and tested a model and compares its prediction to experiment.

One modeling technique for locomotion in complex environments was discrete element method (DEM) simulations [20]. While a reliable method, DEM simulations were computationally intensive. These simulations became infeasible when modeling small grain sizes or long term dynamics. Resistive force theory (RFT) in a multibody dynamic simulation proved a less computationally intensive alternative to DEM simulations while still maintaining predictive accuracy [13]. When modeling more complex robots, however, these engines did not have the capacity to program in controls or different limitations. Motors in these simulated robots were assumed to be infinitely powerful and could achieve the desired motion regardless of constraint forces. This often led to a-physical responses that failed to match the experiment.

To address these simulation challenges, Tingan Zhang, a PhD student in the Goldman group, modeled the bipedal walking robot using the Chrono physics engine that incorporates both RFT and realistic controls for the bipedal robot. In addition, we used this engine to generate resistive forces on the entire foot of different intrusion parameters as a basis for describing bipedal walking behavior.

A contrast between simulation and experiment was the presence of the persistent asymmetry in the experiment. Far from an anomaly to be ignored, this asymmetry provided valuable insights and a simple model with which we understood the differential slip that occurred during bipedal walking in granular media. Using the forces found in simulation, we studied the relative forces that each foot experienced and expanded on this differential slip model.

3.3 Methods

3.3.1 Chrono::Engine

In conjunction with experiments, Tingnan Zhang created a template for simulating the robot using the Chrono::Engine software [67]. The Chrono::Engine was middleware that consisted of a library of C++ objects and functions which were used by third-party developers to conduct complex physical simulations. This software architecture was robust and modular, allowing for different modules to be used depending on the needs of the program. This allowed for an accessible interface when creating

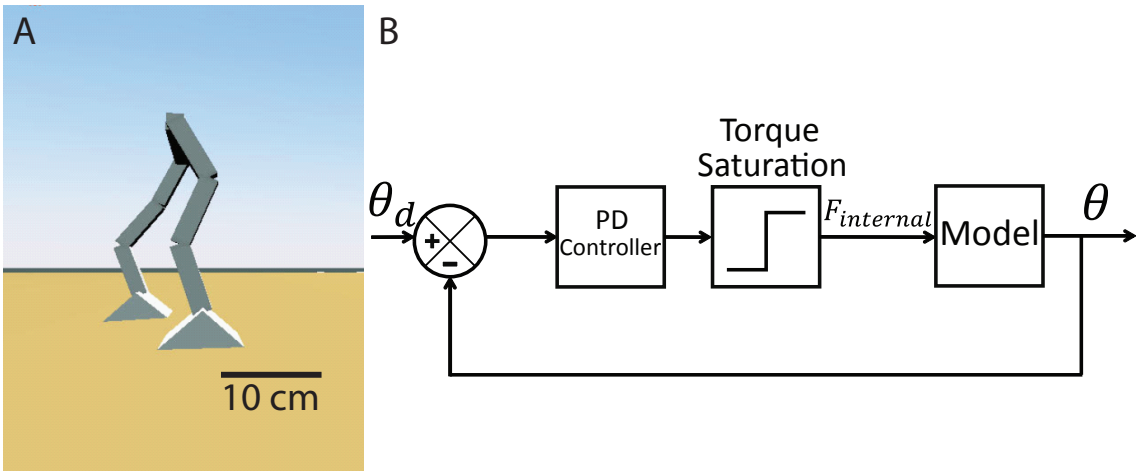

Figure 14: Chrono::Engine RFT simulation. (A) Simulated robot in the Chrono::Engine RFT. It walked with triangular, wedge-shaped feet. (B) Control scheme used to control the joints of the robot in simulation. Modeled off of the motors that the experimental robot used, the desired joint angle was fed into a feedback loop, passing through a PD controller with the same torque saturation limit as the physical motors. These internal forces were fed through the force model and resulted in the output angular position, which itself was fed back again into the system to model the internal motor control.

simulations. Among these optional modules were 3D viewing and animation to render the simulation.

The module-based Chrono::Engine allowed for a multi-body dynamics approach to modeling the robot. Another module was used so the ground reaction forces from the material were from the RFT model [13]. Each segment of the robot was divided into smaller areas of different instantaneous orientation, depth, and direction of motion. The forces on each segment were then calculated and integrated over to determine the forces on each joint and the resultant locomotion of the robot. ϕ was modeled to match experiment by providing a scaling factor to the ground reaction forces. The simulated robot had the same dimensions and mass as the experimental robot and was given the same walking gaits used by the physical model. The mass of the simulated robot was divided uniformly over each segment. As opposed to conical disks, the feet were modeled as wedges of the same area for ease of simulation.

3.3.2 Controls

In previous multi-body dynamic simulations (MBDyn), external forces were derived directly through RFT while internal forces were matched such that the robot attained the desired locomotion [13]. The internal position of each segment was given and internal forces were set to match the desired position regardless of their value. This led to cases where the simulation provided physically unrealistic internal forces and unstable behavior. Noise within the position information led to bizarre results such as the robot launching itself out of the media or sliding forward during the single support swing phase.

Tingnan Zhang simulated the robot used in experiment by instead using a PD controller for each joint to act as the servo motors. The controller took the angular position trajectories used in experiment as input and fed it through the controller to derive the resultant internal forces. The controller passed the calculated internal torque through a torque saturation limit that matched the torque limit on the servo motors used in experiment. This limit kept the simulated robot bound to physically realistic forces to achieve its desired gait. We tuned the gain and damping values so the controller was stable and responsive throughout the simulation. The simulated robot and control scheme is depicted in figure 14.

3.3.3 Simulated foot forces

While RFT was useful as a simulation tool to calculate ground reaction forces on an intruder, its use for providing intuitive insight was more limited. It was not immediately clear how the forces acting on an individual segment reflected on the forces on an entire foot. We expanded RFT with a simulation that modeled just a single foot moving within granular media. These single-foot forces stood as a basis for understanding the ground reaction forces on the robot given its walking gait. However, when expanding RFT to a larger object, we also considered the instantaneous rotation of the object. A foot that rotated in place still had instantaneous directions of motion γ for different segments of the foot. When we considered a foot that was both moving with its own γ at some speed v and rotating with some rotational speed ω,

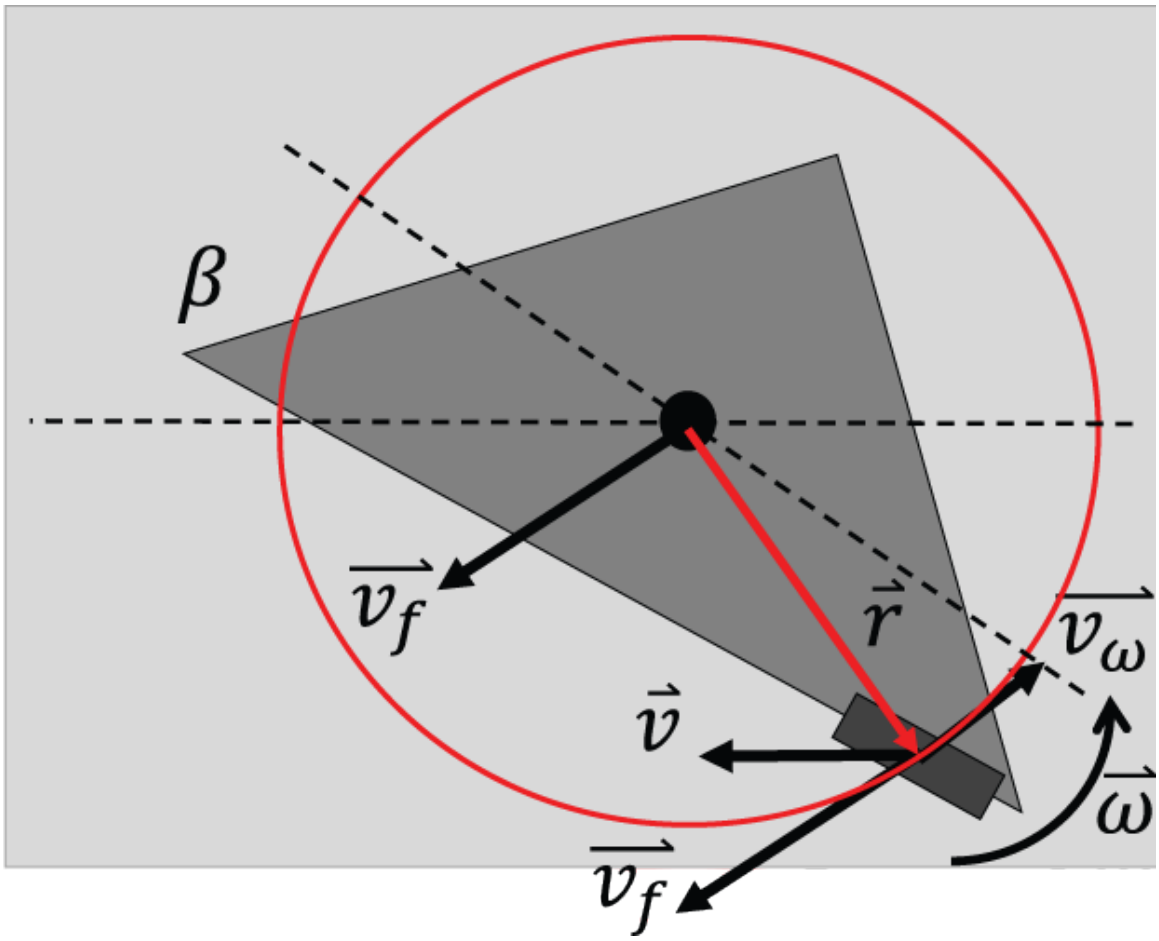

Figure 15: Rotating foot in Chrono::Engine simulation. Effective γ_i of a segment is a function of γ, β, and ν.

calculating the effective direction of motion γ on an individual segment became more complicated. A representation of this scenario is shown in figure 15. We discovered this relationship for an arbitrary segment i on the object through the following equations.

The velocity $\vec{v}_i$ of a segment was described as

$$\vec{v}_i = \vec{v}_f + \vec{v}_{\omega,i} \tag{2}$$

where $\vec{v}_f$ was the velocity of the whole foot and $\vec{v}_{\omega,i}$ was the velocity of the segment from rotation. These velocities were described as

$$\vec{v}_f = v_f \cos(\gamma)\hat{x} + v_f \sin(\gamma)\hat{z} \tag{3}$$

$$\vec{v}_{\omega,i} = \vec{\omega} \times \vec{r}_i(\beta) \tag{4}$$

Since the rotation was planarized, $\hat{\omega} = \hat{y}$, or out of the plane of motion. The position of the segment $\vec{r}_i(\beta)$ was dependent on the orientation β. After fully calculating the effects of this rotation, we defined $\nu = \frac{\omega}{v_f}$ where

$$\gamma_i = \tan^{-1} \frac{\sin(\gamma) + \nu(r_{x,i,0}\cos(\beta) - r_{z,i,0}\sin(\beta))}{cos(\gamma) - \nu(r_{x,i,0}\sin(\beta) + r_{y,i,0}\cos(\beta))} \tag{5}$$

Thus the total foot force was a function of z, β, γ, and ν. We calculated the instantaneous resistive force on the entire foot over a physically realistic range of β, γ, z, and ν.

3.4 Results and discussion

3.4.1 Sensitivity to foot intrusion kinematics

Unlike the experiment, the asymmetry between the two different steps did not exist within simulation. As shown in figure 16, the dependence on foot intrusion kinematics remained with peak step distance again found at presentation angles of 30^o, although the differences were less pronounced with the simulation. Most importantly, the regions of this slip were found at the onset of the two-foot interaction that occurred during intrusion. Until the two feet interacted with the material simultaneously, the step distance was identical to the no-slip condition.

3.4.2 Effects of volume fraction

At low volume fractions, the step distance of the simulated robot was largely insensitive to changes in volume fraction as shown in figure 17. However, for high presentation angles, step distance instead decreased with increasing volume fraction. The changes were ultimately small, but this nevertheless suggested a different mechanism than what occurred within the experiment. The slip experienced during simulation did not occur while the foot was dragged across the material but primarily during the

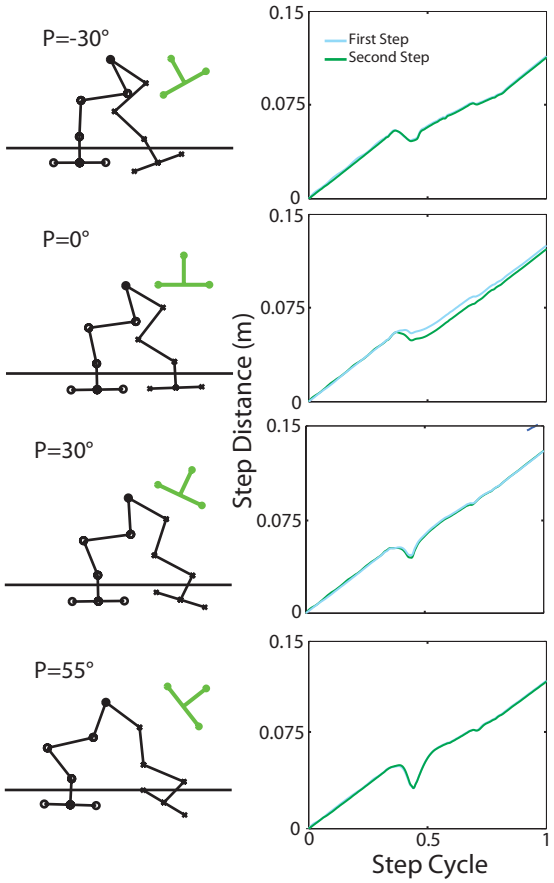

Figure 16: Kinematic performance in simulation across different presentation angles. On the right are step distance vs step cycle (time divided by time of 1 step, 3 s) plots across multiple presentation angles. Images on the left show the position of the robot at the point of intrusion for each presentation angle. As opposed to the experiment, there is no systematic asymmetry between the two steps.

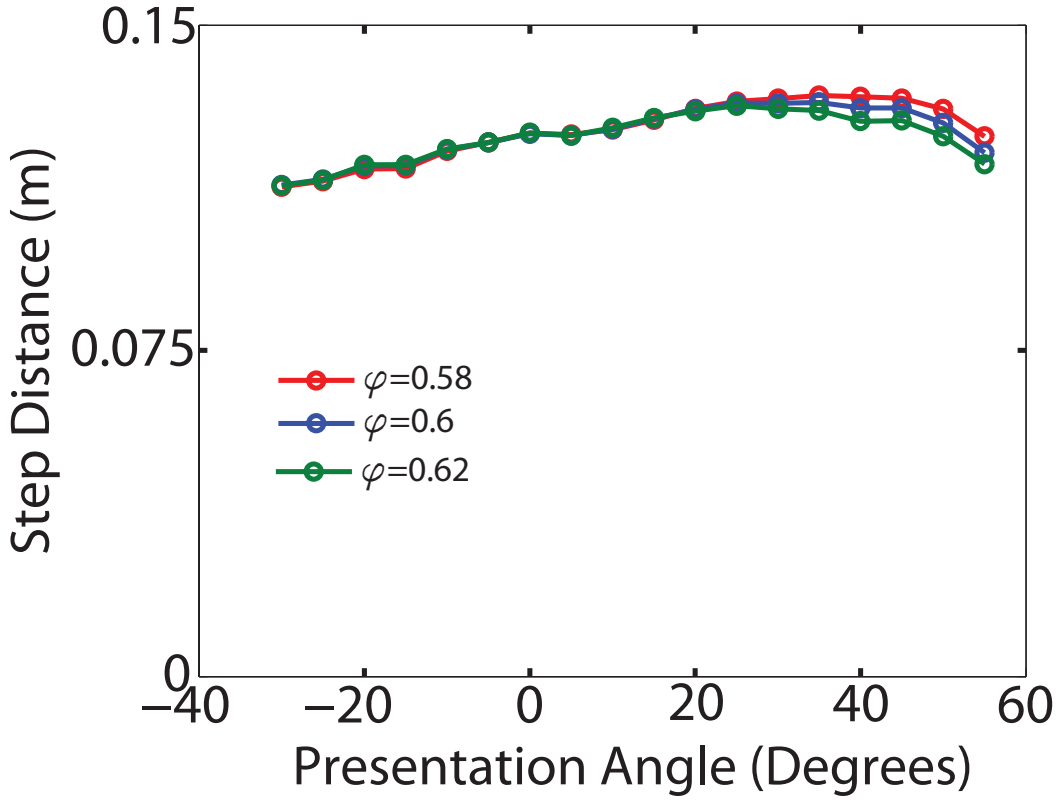

Figure 17: Effect of volume fraction on robot in simulation. Step distance vs step cycle (time divided by time of 1 step, 3 s) across multiple volume fractions. The simulated walker was insensitive to changes in volume fraction outside of higher presentation angles.

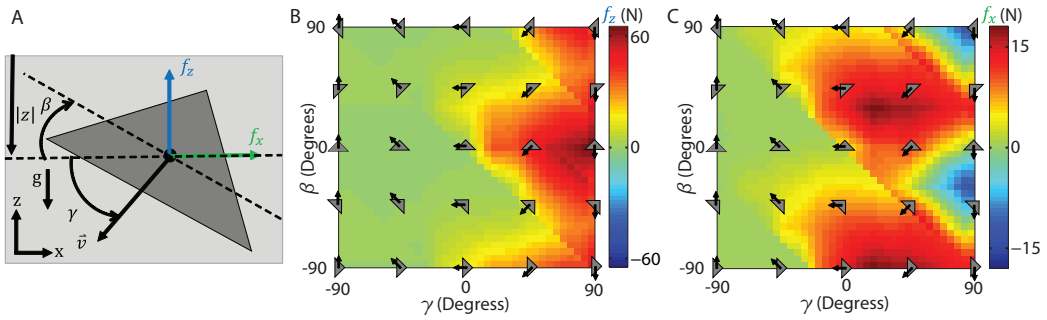

Figure 18: RFT forces for an entire foot. (A) Entire wedge shaped foot 8.5 cm long, 8.5 cm wide, and 7.5 cm tall. The foot is taken as an object of an instantaneous depth z, orientation β, direction of motion γ, and rotational velocity divided by the speed of the foot ν to find the horizontal and vertical forces f_x, z in the RFT Chrono::Engine simulation. (B) and (C) color maps for the foot at $z = 0$ and $\nu = 1$ for the respective vertical and horizontal forces as a function of β and γ. These forces increase and follow a similar profile with increasing depth.

intrusion phase. The higher presentation angle began carrying a negative cost and experienced more slip. The sensitivity observed in experiment may instead be more closely related to the asymmetry.

Despite changes in volume fraction, step performance was only affected during the two-foot interaction of the intrusion phase. This suggests that whatever the mechanism of this slip was, it was independent to changes in the scaling of the ground reaction forces.

3.4.3 Foot forces

It was clear that ground reaction forces were not symmetric about γ for forces on an individual foot: Intruding forces were higher than extruding forces. This dependence on γ diminished as ν increased. Under the proper confluence of parameters, a resistive force in the x direction aligned with that component of the direction of motion. This positive resistive force was a function of the morphology of the foot shape when held at those orientations β. This agreed with other studies which have revealed shape-dependent, drag induced lift forces on an object being dragged through granular media [68]. A representation of these foot forces is shown in figure 18 at the surface for $\nu = 1$.

3.4.4 Intrusion slip

We saw that both the experimental and simulated robots experienced a slipping period where the stance foot slipped backwards that occurred during the two-foot interaction. We defined this amount that the stance foot shifts as the slip S, where negative S was the robot slipping backwards. The onset of this slip took place during the two-foot interaction of the intrusion phase. As the robot walked within the quasi-static regime, the slip was not the result of inertial forces but the interaction between the feet in the granular media. For the overall presentation angle, the forces on the intruding foot were minimized at presentation angle of 30°, which minimized the overall slip on the robot.

3.4.5 Double support slip

We examined the step distance for both simulation and experiment and observed that the simulation largely out-performed the experiment with the exception of presentation angles around 30°. We saw that both the simulated and experimental robots walked successfully over a wide range of volume fractions. The physical robot only failed at large presentation angles of 55°.

The asymmetry in experiment resulted in a double-support slip in addition to the same intrusion slips measured in simulation. Since each limb had a different stride length over the same period, the two feet moved relative to each other even during the double support phase. Granular media, however, exhibited solid-like and fluid-like properties depending on the external forces applied to the substrate. When both feet pushed against each other in the material, the material provided solid-like constraint forces until the stress applied by the foot exceeds the yield criterion. The material behaved as a resistive fluid in this yielding regime and provided ground reaction forces independent of the velocity at low speeds. As long as these ground reaction forces did not exceed the yield criterion of the opposing foot, only one foot yielded through the material while the other remained stationary. During the double support phase, the feet held the same orientation and the ground reaction forces scaled linearly with depth. We therefore predicted that the lower foot remained planted in the material

while the higher foot slipped through the media accordingly.

We defined each foot as either K or G with the center of the robot defined as R. Thus $K_{x,1}$ referred to the x-position of foot K at the end of the double-support phase for the first step (immediately before the onset of extrusion of the back foot) while $R_{x,2}$ referred to the x position of the center of robot during the same phase of the second step. During a step, the displacement of the stance foot was defined as the slip experienced during intrusion, S_I, and any slip experienced during the traditional double support phase, S_D. A representation for this slip is shown in figure 19. By working through these definitions, we were left with the following equation for the two cycle displacement given the relative height of each foot.

$$R_{x,3} - R_{x,1} = \begin{cases} (K_{x,3} - K_{x,2}) + S_I & \text{if } G_{z,2} < K_{z,2} \;\&\; G_{z,3} < K_{z,3} \\ (G_{x,2} - G_{x,1}) + S_I & \text{if } G_{z,2} > K_{z,2} \;\&\; G_{z,3} > K_{z,3} \\ \frac{(G_{x,2}-G_{x,1})+(K_{x,3}-K_{x,2})}{2} + S_I & \text{if } (G_{z,2} > K_{z,2}) \;\&\; (G_{z,3} < K_{z,3}) \\ & \text{or } (G_{z,2} < K_{z,2}) \;\&\; (G_{z,3} > K_{z,3}) \end{cases} \tag{6}$$

Therefore, we understood bipedal walking in granular media by understanding the two-foot interaction that took place during intrusion and the double support phase. The foot with the greater predicted drag force remained stationary while the other foot slipped and yielded through the material. Coupling this slip with the no-slip kinematics of the walker's gait, we predicted the overall motion of the biped in the granular media as shown in figure 20. We measured the depth difference between the two feet from webcam video, defined as the the difference in depth between foot K and foot G immediately before the extrusion phase for each step, or $K_{z,i} - G_{z,i}$, where i was the step number. We incorporated the values of this depth difference, the step length measured in experiment, and the intrusion slip S_I measured from simulation with the above equation to predict the two step displacement and compared against experiment. The model and experiment agreed well across presentation angles.

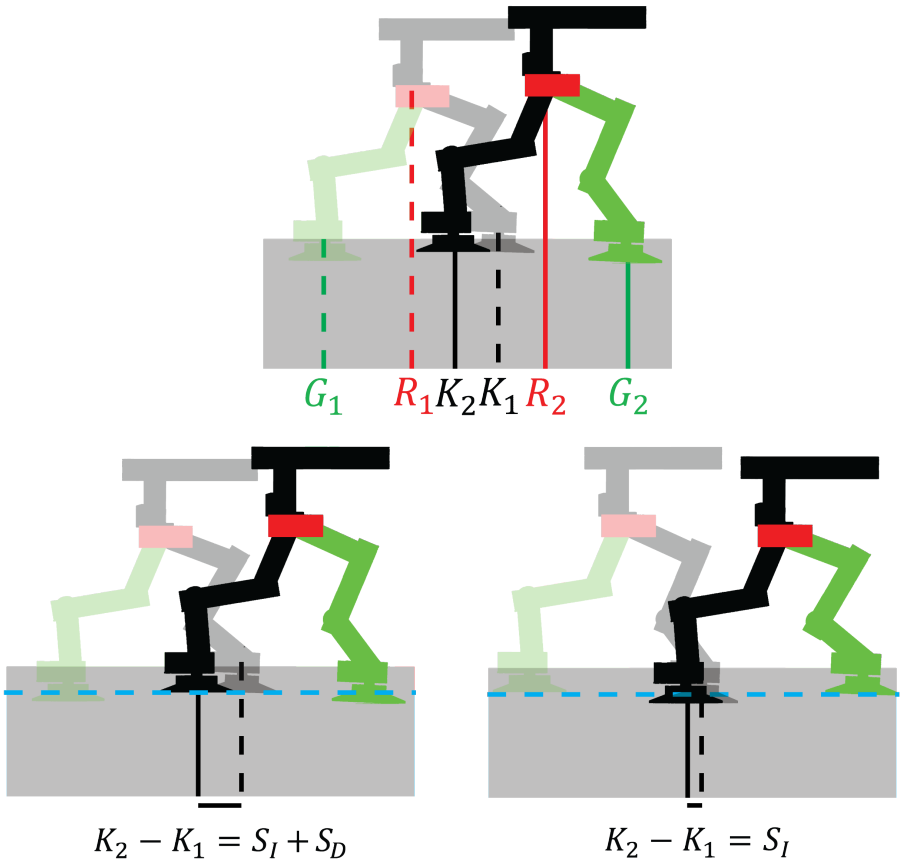

Figure 19: Foot slip in experiment. The robot walking in granular media with the center of the robot shown in red (R) and each leg shown in black (K) and green (G). (A) One step is shown from the robot with the robot shown just as it begins to extract its back foot from the material before and after the step. Its foot positions are shown with indices denoting before the step (1) and after the step (2). (B) The slip experienced ($K_2 - K_1$) for the robot when the intruding foot steps deeper into the material than the back foot while (B) shows when the intruding foot steps higher in the material. When the intruding foot steps deeper into the material, the slip experienced is the sum of the slip during intrusion (S_I) and the difference between the stride length of each step (S_D). When the intruding foot steps shallower into the granular media than the back foot, the slip experienced only derives from the intrusion slip.

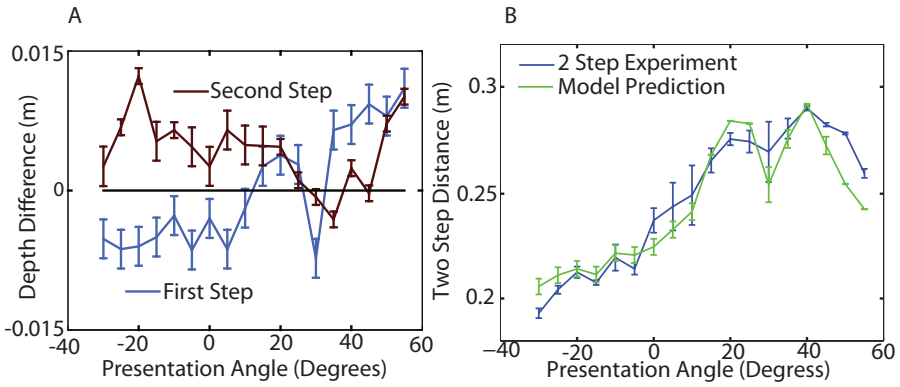

Figure 20: Asymmetry in robot led to differential slip. (A) shows the depth difference vs presentation angle of both feet immediately before the extrusion phase for each step. Positive values indicates one foot being higher in the material while negative values indicating that foot standing deeper in the material. When both lines are positive, the same foot stepped consistently higher in the material as opposed to alternating with each step when the lines are positive and negative. (B) Plots the two step displacement for both the model and experiment with good agreement between the two.

3.4.6 Insensitivity to volume fraction

This differential slip also informs why both experiment and simulation were insensitive to changes in volume fraction and the experiment was insensitive to changes in foot area. What determined whether or not the stance foot slipped in granular media was not the magnitude of the ground reaction force but whether or not the force on the intruding foot exceeded that of the stance foot. Scaling the total ground reaction force experienced by the foot, whether through changes in compaction or in foot area, corresponds to proportional change in the opposite foot. Which foot would slip and when that foot would slip therefore remained unchanged with the scale of the ground reaction forces.

3.4.7 Foot force comparison

The error of the asymmetry in experiment also provided valuable insight into the slip experienced during the intrusion phase. In intrusion phase, the robot's feet both interacted with the ground and also moved relative to each other. The foot that yielded through the material was therefore the foot with the smaller ground reaction

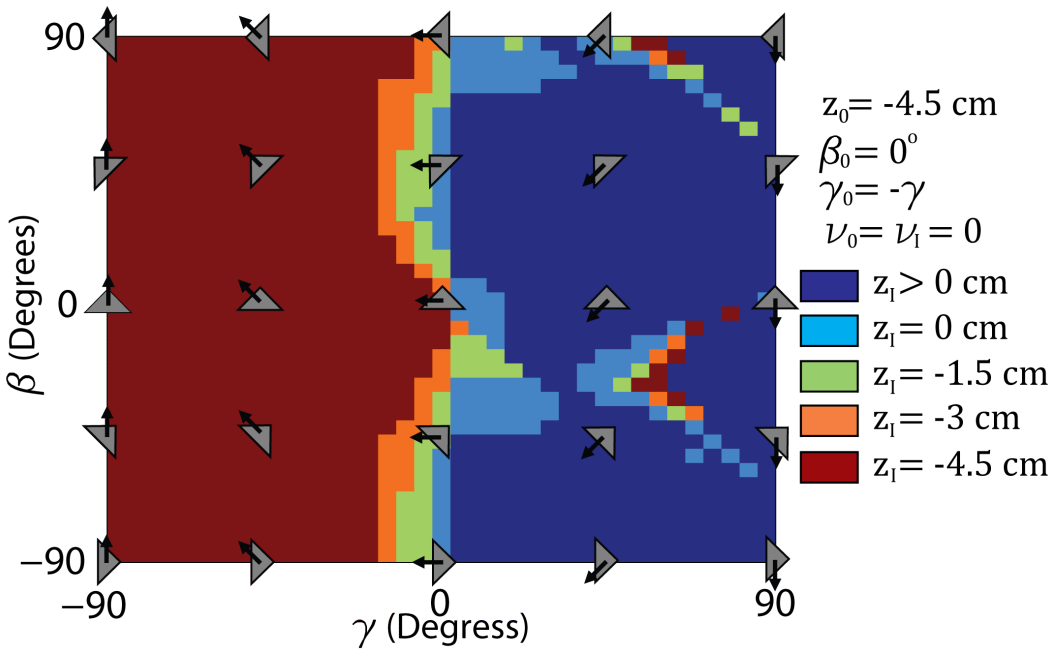

Figure 21: Paths of foot placement without slip. Shown are the regions where the the magnitude of the horizontal force for a foot at orientation $\beta_0 = 0^o$, $\nu_0 = 0$ as $\omega_0 = 0$, and depth $z_0 = -4.5cm$ exceeds the horizontal force of a foot at different depths z_I, orientation β_I, and direction of motion γ_I but for undefined ν_I as $\omega_I = 0$. With each foot moving quasi-statically, the direction of motion of the planted foot is equal and opposite to the intruding foot, $\gamma_0 = -\gamma_I$. As forces increase with increasing depth, each region of higher depth encompasses all regions of lower depth. When the magnitude of horizontal force on the planted foot exceed the force of an intruding foot, the planted foot will not slip and the intruding foot will yield through the material. Thus this figure portrays the regions where a bipedal walking robot would experience no slip while walking in granular media.

forces acting on it. Predicted instantaneous forces on each foot collected in simulation determined which foot yielded through the material at each instant in time.

For regions where the feet moved relative to each other during the two-foot interaction, the feet experienced different resistive forces as predicted by RFT. RFT was defined for continuously yielding material, however. Therefore these RFT forces did not necessarily predict the force a foot experienced while it yielded through the material but also the yield criterion of that foot. Thus the foot with higher predicted resistive forces instead experienced solid-like constraint forces equal and opposite to the resistive force acting on the other foot as it yielded through the material.

This model revealed the insensitivity to volume fraction that we observed earlier. While ground reaction forces scaled with increasing ϕ, these forces scaled proportionally to both feet. Therefore the magnitude of the forces changed but the relation between them did not. During the two-foot interaction, the same foot slipped through the material. The foot with the higher predicted resistive force remained stationary and planted in the direction of motion as the other foot yielded through the material according to their relative motion. When we examined a walking gait, the relative motion of each foot set the appropriate parameter for the direction of motion γ, where the $\gamma_1 = -\gamma_2$.

We compared these forces (shown in figure 21) and discovered why the two-foot interaction only caused regions of slip during the intrusion and double support phases but not during the extrusion phase. Ground reaction forces were not symmetric about the angle of intrusion γ: Forces in the x direction increased as a foot intruded into the material. When the a foot lifted from the material, in contrast, the material provided lower reaction forces for the same β, z and ν. Since the relative forces dictated the differential slip, positive γ of intrusion also reflected that the stance foot had a more negative effective γ. Even at higher depths and therefore lower ground reaction forces, the preference for the direction of motion still brought regions where the force of the intruding foot exceeded the force of the stance foot and caused negative slip. In contrast, extraction provided this advantage to the stance foot and made the robot robust to slipping in this phase. For the double support phase, the two-feet were on equal footing as $\gamma \approx 0$ for both feet. The determining factor for which foot slipped was the difference in the relative height of each foot and whatever rotational motion (if any) it was undergoing.

While we constructed gaits to walk without slip by following intrusion trajectories shown in figure 21, we also created walking parameters to walk without slip regardless of the material properties. This slip only occurred during relative foot motion during the two-foot interaction in the material. We eliminated this relative motion with gaits that placed the foot straight down during intrusion.

3.5 Conclusion

The asymmetry in experiment revealed the underlying principle of differential slip in granular media. When the feet moved relative to each other, the foot with the higher predicted RFT forces remained stationary while the other foot slipped and yielded through the material. This slip was dependent on the foot intrusion kinematics but was largely insensitive to changes in volume fraction as higher ϕ scaled ground reaction forces and had little impact on the relative forces that dominated the differential slip.

We described the double support slip seen in experiment as the differential slip that occurred from the fluid-like and solid-like properties of granular media. The asymmetry provided an easily understood and tested model that described not just the slip during intrusion but all interactions between the feet and the granular media. We found good agreement between this slip model and experiment. We applied this model as a base for creating gaits to walk in granular media without slip regardless of material properties.

CHAPTER IV

BALANCING IN GRANULAR MEDIA

4.1 Summary

We studied bipedal walking in simulation using Resistive Force Theory to understand basic strategies for stable, open-loop, quasi-static walking in granular media. Building from previous research on slip in granular media, the simulated robot walked with a slipless gait. Stable walking with the simulated robot was sensitive to the trajectory of the center of mass during the gait.

We applied insights gained from walking in simulation to a human scale, humanoid robot, HUBO. HUBO was unable to even stand in poppy seeds with its normal feet and instead required larger feet to increase stability. Even with adapted feet, HUBO was unable to walk in granular media with a gait that was stable on hard ground. We adapted a successful gait strategy from simulation to the HUBO robot and achieved successful, open-loop walking in granular media.

4.2 Introduction

While bipedal walking with robots has advanced for efficient robots [69] and robots that walked across uneven terrain [70], deformable media such as loose sand and mud remained a challenge. This challenge stemmed from the lack of comprehensive force laws that described the material. However, advancements in physics have led to empirical force models that accurately predicted the resistive forces from a range of granular media [13].

Hard ground, quasi-static walking was built on inverted pendulum models. These models controlled the torque on a foot-pendulum contact such that the net torque was zero [50]. This was referred to as the zero moment point (ZMP), which was the same as the projection of the center of mass onto the plane of the foot when the height of the center of mass remained constant [71]. The ZMP model maintained

stability as long as the projection of the center of mass was contained within the polygon of support, which was the shape of the foot's contact with the ground. A stable hard ground gait was achieved by keeping the center of mass above the stance foot during the swing phase and shifting it over to the new stance foot during the double support phase. In physical robots, there was an additional torque limit given the constraints of the actuator. Given a limited maximum torque for the actuator, the effective polygon of support shrank. As with physical motor constraints, compliant terrain such as granular media carried a torque constraint not of the motor but of the material: when the external stress on the material exceeded the yield criterion, the ground yielded to the foot and the pendulum became unstable. This relationship is depicted in figure 22.

This Resistive Force Theory for granular media was an empirical-based force model that described the forces on an intruding object as it moved through the material. This model lacked a smooth set of equations that control models rely on, making it better suited for numerical simulations than analytical models. We therefore built on the Chrono::Engine with Resisitive Force Theory to gain insight into walking in granular media and the necessary strategies for open-loop, quasi-static walking. We then tested the insights gained from simulation on a human scale humanoid robot, HUBO [14], to stably walk in poppy seeds.

4.3 Material and methods

4.3.1 Pitching simulation

We used the Chrono::Engine [67] with RFT forces [13] to simulate the robophysical bipedal robot walking in granular media. We conducted additional hard ground simulations where we modeled the ground as an infinitely rigid surface. While the experimental robot was planarized by a set of air bearings to walk on granular media, the simulation removed the in-plane pitch constraint while still constraining it in both roll and yaw. These constraints allowed us to examine the stability of the robot while reducing the number of degrees of freedom and simplifying the walking gaits.

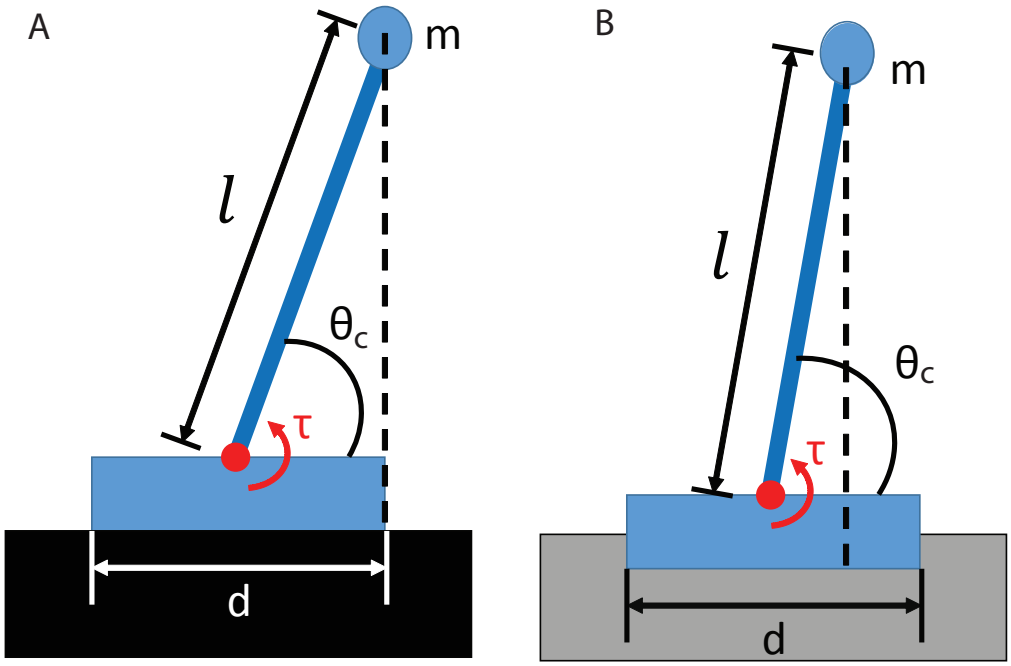

Figure 22: Inverted pendulum model for hard ground and granular media. (A) A massless rod of length l has mass m fixed at the end and attached to a foot of width d. For controlled torque τ, the pendulum remained stable when the projection of the center of mass remained within the area of the foot. Thus the pendulum was stable for angles above θ_c. (B) In granular media, θ_c increased from the granular media's effective torque limit: When the stress of the foot exceeded the yield stress of the material, the ground deformed beneath the foot and the pendulum became unstable.

The simulated robot walked with preset trajectories specifying the angular position of each joint. The robot tracked these angular positions exactly with forces calculated with each time step in simulation to achieve the desired position. We removed the PD, torque saturated controller from previous simulations to achieve the exact commands as the simulated robot's stability was sensitive to slight deviations from the commanded position.

The simulated joint trajectories were calculated from setting the planar position of each foot, their orientation, and the center of mass position in the direction of motion for each leg. Each leg had 4 degrees of freedom and 4 constraints so angular position of each joint was solved directly using a MATLAB solver. These constraints limited the range of achievable motion for the robot, resulting in stride lengths significantly smaller than the size of the foot (8.5 cm long foot, 2 cm stride length). Each gait tested walked with level feet and identical rectangular foot trajectories. There was an adjustment during the intrusion such that there was no relative motion between the two feet in the direction of walking. Without this two-foot interaction from the relative motion of the feet during the intrusion and double support phases, the simulated robot walked without slip.

The gaits varied the position of the center of mass in the direction of motion. We tested walking gaits with the center of mass close to the center of the robot (Central gait), the center of mass held at the center of the stance foot and transitioned between the two feet during the double support phase (Hard Ground gait), and shifted the center of mass to the intruding foot half way through intrusion (Shifted gait). These gaits are all portrayed in further detail in figure 23.

We additionally studied the effects of foot width on these walking gaits in simulation. We simulated foot widths ranging the 8.5 cm used in previous simulations to up to 6 times wider with a feet 51 cm wide. Each simulation used the same foot length of 8.5 cm. RFT forces scaled linearly with the area so the ground reaction forces scaled proportional to the foot width.

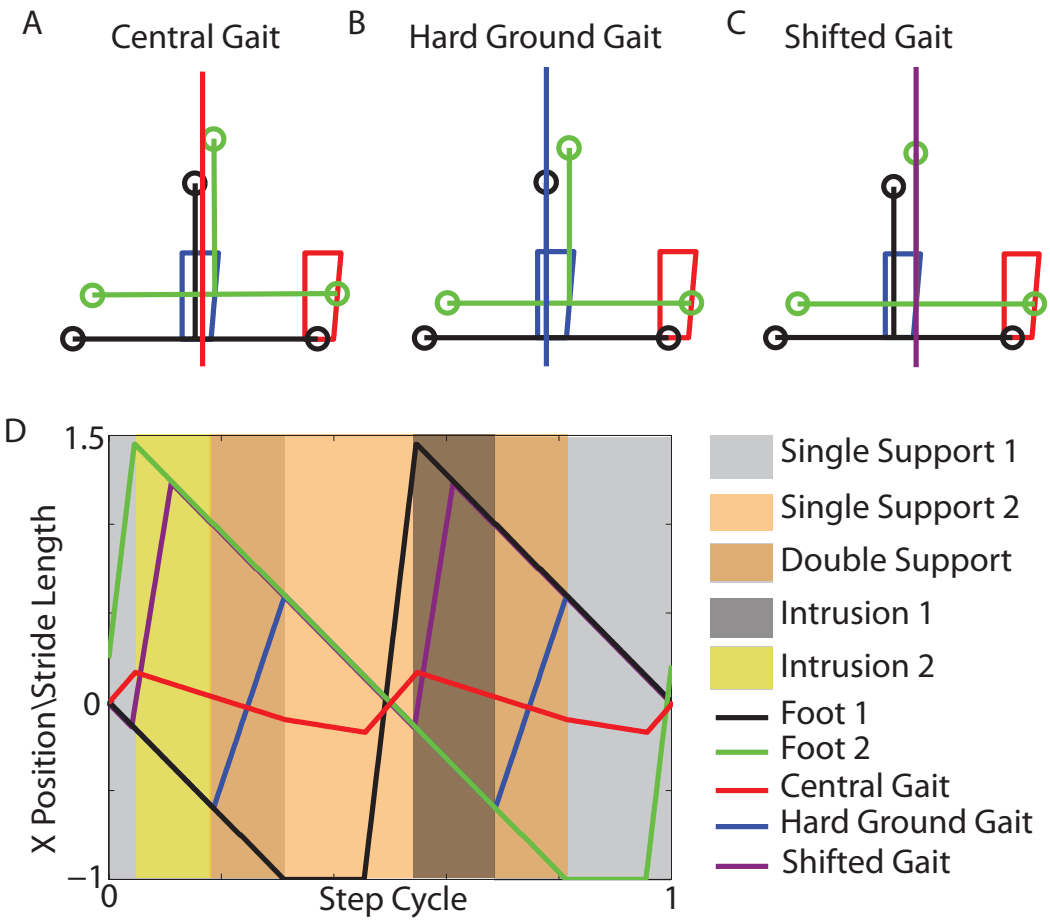

Figure 23: Walking gaits used in Chrono::Engine simulation. (A), (B), and (C) show the position of the center of mass and the feet of the respective Central, Hard ground, and shifted gaits. Each gait moves with the same red and blue trajectories for the tip and center of the foot but with different center of mass control. (D) shows the x-position of the center of mass of each gait relative to the foot trajectories. The intrusion, single support, and double support phases are highlighted.

4.3.2 HUBO Robot

In collaboration with Prof. Aaron Ames, we conducted experiments using the HUBO-1 robot. The HUBO-1 robot was a human scale humanoid robot developed by KAIST [14]. HUBO was designed for efficient bipedal walking by using low power motors to move. HUBO had 41 degrees of freedom, weighs 50 kg, and is 1.2 m tall. HUBO walked with aluminum rectangular feet 22.9 cm long and 15.2 cm wide.

The HUBO robot was supported by a steel gantry system with support ropes hanging slack during the experiment to catch HUBO when it fell so as not to damage the robot. In conjunction with Dr. Christian Hubicki, a postdoc with Prof. Ames, we constructed a rectangular bed of poppy seeds 2 m long, 1 m wide, and 0.3 m deep and filled the bed with 180 kg of poppy seeds. After each trial of the robot walking in the poppy seeds, HUBO was hoisted off the surface from a winch attached to the gantry system while the bed was manually reset by raking the poppy seeds to a smooth, level surface. The full experimental apparatus is shown in figure 24.

We clamped wooden boards of varying widths (22.9 cm long and from 17.8 cm to 30.4 cm wide) to the bottom of HUBO's feet for stability tests and walking on granular media. We cut an additional board of the maximum size with a rectangular hole cut from the center. This cut foot had the same polygon of support on hard ground but half the surface area of the largest width foot. HUBO was controlled with an adjustable open-loop gait created by Michael Grey, a PhD student with Prof. Ames' group, to walk without slip in granular media.

4.4 Results and discussion

4.4.1 Foot stability

In simulation, the bipedal robot walked successfully on hard ground for each tested gait. This result agrees with ZMP models as the projection of the center of mass of each gait was contained within the stance foot. In granular media, the robot was sensitive to the center of mass position even during the swing phase. RFT was built for intruders continuously yielding through granular media and did not take static forces into account. Therefore, when the center of mass was not positioned perfectly

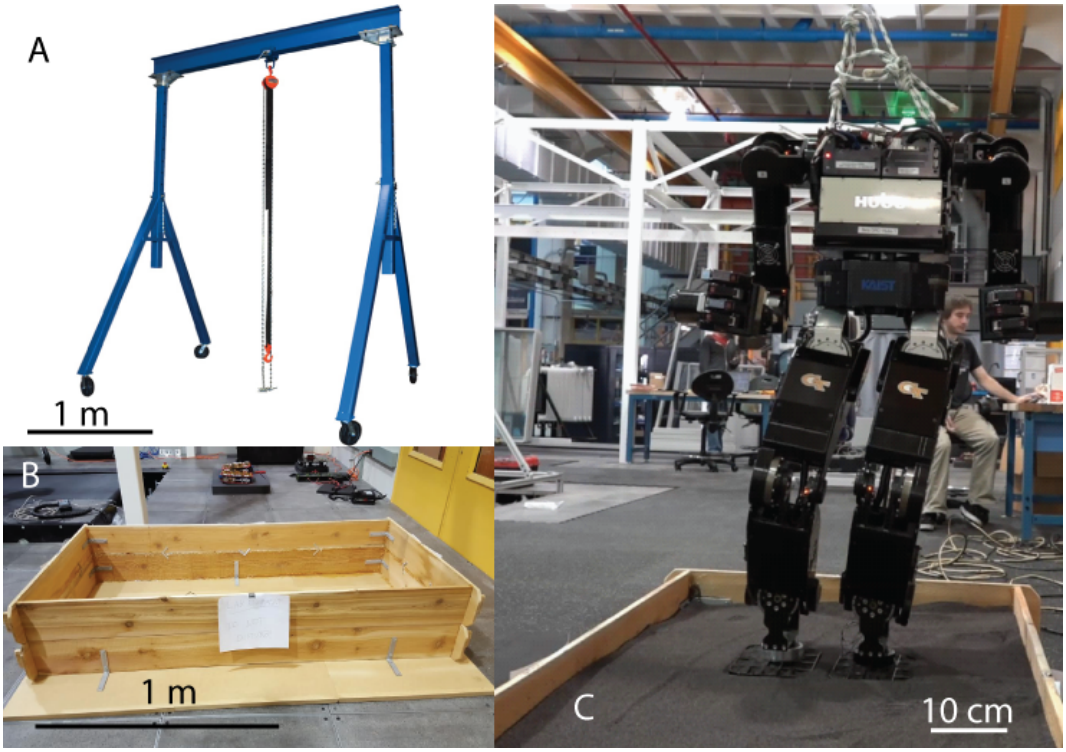

Figure 24: HUBO experimental setup. (A) Steel gantry system used to catch HUBO in case of a fall. (B) Wooden test bed containing the poppy seeds for HUBO to walk in. (C) HUBO robot standing in poppy seeds.

above the center of the foot, numerical errors accumulated in simulation such that the robot would pitch. The rate of this pitch decreased with larger feet and the increased with greater difference between the position of the center of mass and the center of the foot. As such all of the tested gaits still walked successfully through the swing phase without falling.

The HUBO robot fell immediately when placed in the granular media. Additional tests revealed that the HUBO robot was unstable and could not be placed to stand on one foot. Slight variations in how HUBO was placed onto the material affected in which direction HUBO would pitch in the first place. This failure maintained despite adjustments to the center of mass position of the robot. We then expanded the effective area of HUBO's foot by clamping on boards of varying width, up to twice the width of HUBO's natural foot. Only when equipped with an up to 50% larger foot did HUBO stand stably on one foot in the poppy seeds, as shown in figure 25.

In hard ground a larger foot corresponded directly to increasing in the polygon of support. From the ZMP model, the robot was stable as long as the projection of the center of mass was contained within this polygon of support (see figure 22). In granular media, however, the polygon of support was not the relevant factor. We tested the HUBO robot with two feet of different area but the same polygon of support as shown in figure 25. HUBO stood stably on the foot with the larger area and could not stand on the smaller foot.

Previous experiments in bipedal walking in granular media revealed the importance of the solid-like and fluid-like properties of the material as they pertained to the differential slip. During the single support phase, the planarized robot simply sank to a depth in the material where the substrate provided solid-like constraint forces that did not exceed the yield criterion [11]. Without this planarized constraint, the yield criterion of the material extended beyond the translational forces and applied to external torques as well. While hard ground bipedal walking considered torque limits for the actuator in constraining the center of mass position, here we considered torque limits for which the material could support the robot without yielding.

The HUBO robot therefore could stand successfully with larger feet as the stress

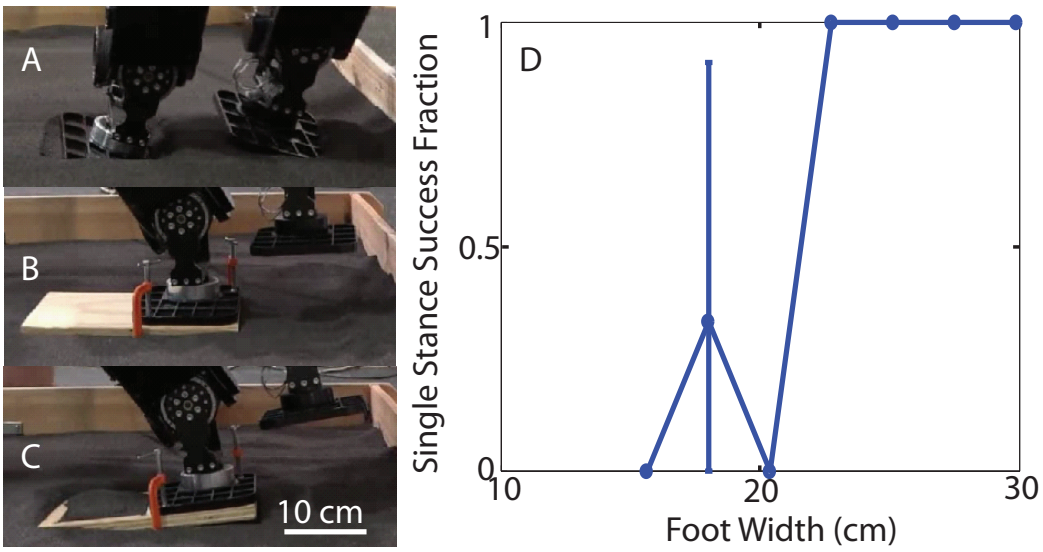

Figure 25: HUBO static balancing in granular media vs. foot width. (A) shows HUBO failing with its natural foot while (B) shows a stable stance with a foot twice as wide. (C) shows an unstable stance with a foot of the same width as (B) but half of the surface area. (D) Stability vs foot width in granular media, where HUBO was unstable with smaller feet. The error bar indicate one of the three trials was successful at 17.78 cm foot width while all other trials had the same results for that foot width.

of the robot was spread across the material did not exceed the yield stress of the material. From RFT, we understood increasing the yield stress as increasing the ground reaction forces of the material. This stability with larger foot width was the functional equivalent increasing the volume fraction, ϕ.

4.4.2 Effect of center of mass trajectory on gait stability

While the simulated robot did not fall during the stance phase across the tested gaits, the Central and Hard Ground gaits failed during the two-foot interaction that occurred during intrusion (as shown in figure 26). The robot experienced additional torque as the intruding foot entered the material which pitched the robot backwards. Both Central and Hard Ground gaits monotonically improved performance with increasing foot width. The benefit of larger foot size was two fold: First the wider feet increased ground reaction forces and slowed the rate of pitching as seen in single support tests. Second the robot did not sink as deep into the material, resulting in

a shorter and less impactful intrusion phase. As the foot width increased the ground reaction forces approached solid-like properties.

The Shifted gait walked successfully for several cycles although this success depended sensitively on the timing of the shift. While both Central and Hard Ground became more stable with increasing foot width, the Shifted gait improved stability with larger foot sizes until it transitioned from pitching backwards to pitching forwards. As foot sizes increased further, the performance of the Shifted gait decreased until the ground reaction forces approached solid-like properties. Around the transition from pitching backwards to pitching forward, the ground reaction forces were roughly equivalent. The dominant factor was the point in the cycle the robot begins to interact with the material relative to the shift. Shifting the center of mass forward during intrusion minimized the torque on the robot and increased stability. Performance dropped as the foot width increased further and the shift occurred before the foot interacted with the material. At this stage the robot became unstable during the single support phase and began to pitch forward.

We tested the HUBO robot with the 30.4 cm, single foot-stable feet in the poppy seeds. Walking gaits that were successful on hard ground failed after a step or two with the robot pitching backwards. As shown in figure 26, we tested shifted gaits where the robot began to shift its center of mass at a point during its intrusion phase to an amount of the distance between the stance foot and the intruding foot. Given limitations for the robot's range of motion, we fixed the amount to shift constant at 30% and instead changed the timing during intrusion when the center of mass started shifting. At 60% during intrusion, HUBO pitching backwards during the two-foot interaction. At 70% and 80% shift, the robot also pitched backwards after a step from the torque experienced during intrusion. At 65% the HUBO robot took several strides without falling.

The results with HUBO agreed with simulation. Walking in granular media became more stable with increasing foot width. Additionally, stability sensitively depended on the timing of shifted gaits.

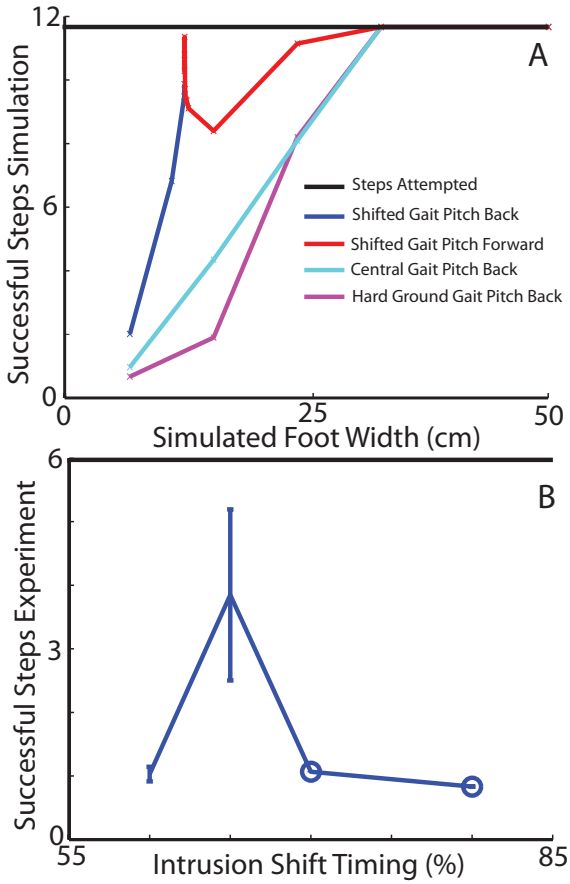

Figure 26: Stability during locomotion in simulation and experiment. (A) Number of successful steps vs. foot width for Central, Hard Ground, and Shifted gaits. Both Hard Ground and Central gaits pitched backwards across trials and improved stability as foot area increased. The shifted gait also generally improved stability as foot width increased but showed sensitivity to the timing of its gait around higher stresses as it transitioned from pitching backwards to pitching forward. (B) Number of steps vs. gait timing in HUBO robot. HUBO was sensitive to this timing and only could take multiple steps at a shift starting 65% through intrusion. 70% and 80% lack errorbars as they were single trials.

4.5 Conclusion

We built on previous simulations to study balance and pitch in bipedal walking in granular media. We used our understanding of the solid-like and fluid-like behavior of granular media to understand the stability of the material. We demonstrated that increasing stability was a function of decreasing the external torque or increasing the yield criterion of the media. Finally we applied insights gained from simulation to the HUBO robot walking in poppy seeds to have it walk successfully without slip in an open-loop cycle.

CHAPTER V

CONCLUSION AND FUTURE WORK

5.1 Conclusion

In this dissertation, we used the methods of robophysics to create a fully automated bipedal robot and systematically explored effects of limb intrusion kinematics, volume fraction, and foot size on the performance of walking in granular media. We uncovered the underlying physical principle that described the overall performance of this locomotion: differential slip experienced during the two-foot interaction.

To compare the findings of this physical robot to previous work on legged locomotion in granular media, we simulated the biped using the Chrono::Engine with ground reaction forces from RFT. The Chrono::Engine simulation allowed for direct comparison between experiment and simulation as the motors used in simulation were physically tuned to match the controls and torque saturation limits used by the servo motors in experiment.

We observed that the differential slip in simulation and experiment occurs when the two feet move relative to each other within the granular media. We demonstrated that the foot that has higher predicted drag forces from RFT remained stationary while the other foot yielded through the material. This was a result of the fluid-like and solid-like properties of granular media where the material remained solid and provided constraint forces until the yield criterion was met and the material began to flow. When we compared two feet that moved relative to each other within the material, the foot with lower predicted drag forces yielded through the material while the the other foot remained stationary.

We expanded the simulation to allow the robot to pitch and studied balancing in granular media. The fluid and solid-like properties of granular media once again determined stability in the substrate: When the external torques exceeded the yield criterion of the material, the walker became unstable. We tested these principles on

a humanoid scale robot, HUBO, and HUBO walked successfully in granular media from insights gained from this model.

5.2 Future work

5.2.0.1 Gait optimization

Robophysics is an iterative process that improves both physics and robotics. While we have used robots to explore the physics of walking in complex material and have improved robots to successfully walk in these environments, we will continue to iterate through this methodology. We will incorporate our model for the granular media in control methods that optimize walking gaits given a physical model [72]. In efforts to discover ideal walking gaits, this optimizer will test the bounds of our model and reveal areas where our model prediction does not agree with the robot's performance. This serves to highlight areas to further explore and improve our understanding of physics, which in turn improves our ability to control robots.

5.2.0.2 Foot morphology allowing preferential slip

In addition to continuing the process of robophysics through gait optimization, we will also explore the effect of foot shape on walking in granular media. We will investigate foot designs that preferentially slip in one direction over the other. With a different foot shape, we will reduce the forces of intrusion while increasing the forces that the stance foot experiences. By changing the shape of these force relations in the direction of motion, higher relative forces for the stance foot mean that the biped would experience less negative slip. These advantages are gained without any change to the controller.

5.2.0.3 Differential slip in worm locomotion

While this dissertation has explored the effect of differential slip in bipedal locomotion in loose material, this does not mean that this principle is unique to this system. The FlipperBot [34], for instance, experienced the differential slip between the intruding fins and the drag from the body of the robot.

This principle of differential slip is not constrained to legged-locomotion. Worms are ubiquitous organisms that exist in soils of different properties across the world [73]. Many of these worms move through a peristaltic process: The head of the worm contracts and pushes forward through the material while the back remains anchored [74]. After extending the head, the worm then expands its head while pulling its back forward through the material and repeating the process. This two-anchor system is explained through differential slip. By expanding or contracting the head, the worm controls the effective maximum drag forces that that portion of the body will experience within the substrate. It effectively anchors one portion of its body so that the material provides solid-like constraint forces and pushes or pulls the rest of its body through the fluid-like material providing resistive forces.

To test this form of locomotion, a simple worm-inspired robot was built by Lillian Chen, an undergraduate student in the Goldman group. We constructed this robot with a set of linear motors. Two carriages were attached at the end of a linear motor. Each carriage itself housed two perpendicular linear motors pointed in opposite directions that pushed out or contracted a plate from the carriage. This motion controlled its effective area with respect to the surrounding substrate. We tested this robot in a model substrate of 3 mm plastic particles where the worm robot was able to use these motors in a form of peristaltic locomotion to advance within the material. As opposed to the bipedal walking robot that stepped into undisturbed material, this worm-inspired robot interacted with previously disturbed material. As such predictions from RFT broke down during surface locomotion as swaths of disturbed material provide different resistive forces than otherwise predicted.

Future testing will examine this worm-inspired robot in a cohesive granular media as shown in figure 27. Hollow 3D printed plastic particles of 1.8cm diameter were printed in male and female halves that screwed together. A cubic neodymium iron boron magnet (0.635 cm side, N48 strength) was placed in each particle and screwed together. The bulk material had known cohesive granular properties. The large size of the particles allows for the particles to be reasonably modeled in DEM simulation.

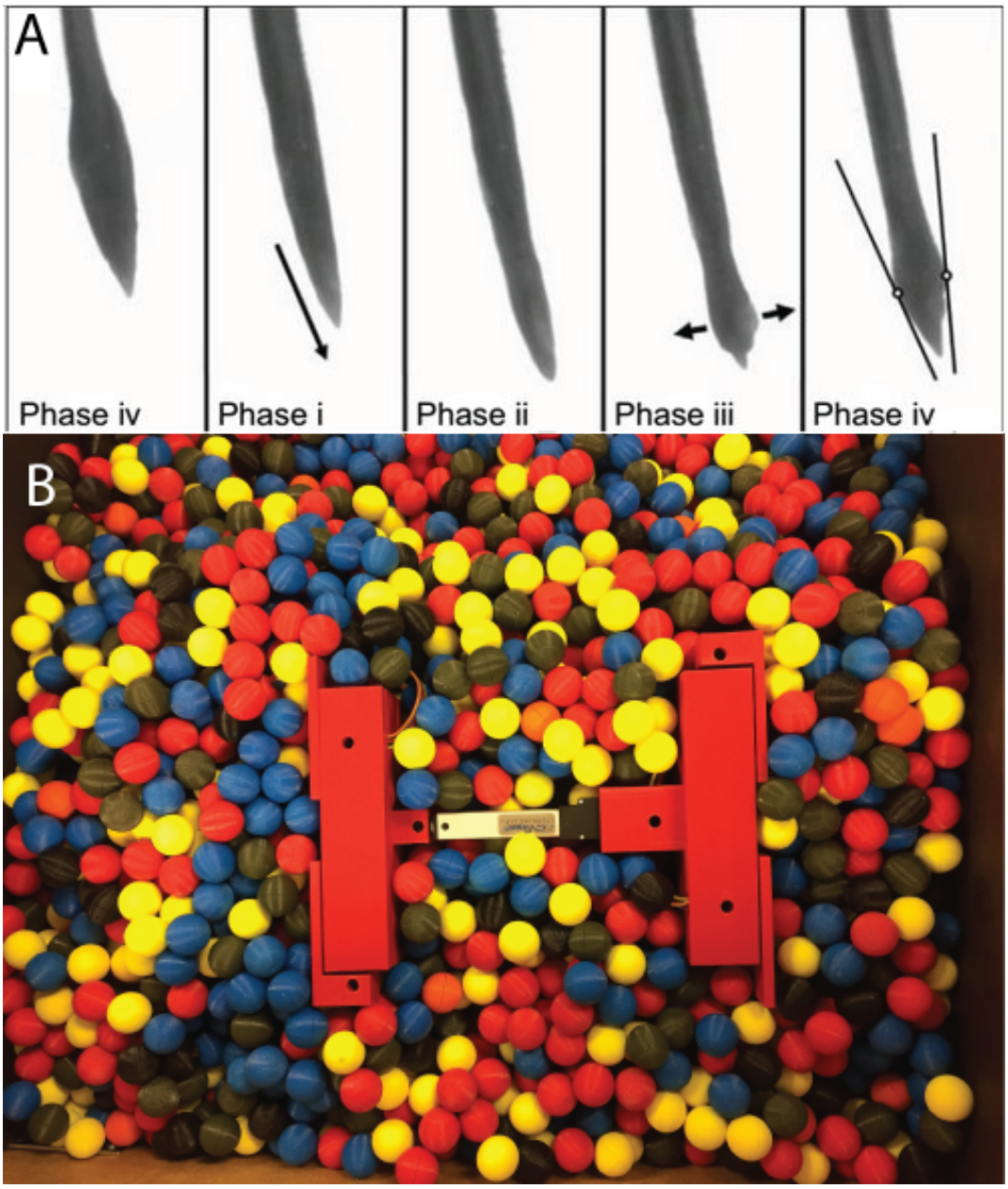

Figure 27: Worm locomotion and worm-inpsired robot in cohesive granular media. (A) Phases of worm locomotion. Worm contracts and pushes forward its head, then expanding the head after fracturing the material and pulling its body forward [74]. (B) Worm-inspired robot in 3D printed magnetic particles.

REFERENCES

[1] Jennifer Casper and Robin Roberson Murphy. Human-robot interactions during the robot-assisted urban search and rescue response at the World Trade Center. *Systems, Man, and Cybernetics, Part B: Cybernetics, IEEE Transactions on*, 33 (3):367–385, 2003.

[2] Steven W Squyres, Andrew H Knoll, Raymond E Arvidson, James W Ashley, JF Bell, Wendy M Calvin, Philip R Christensen, Benton C Clark, Barabara A Cohen, PA De Souza, and others. Exploration of Victoria crater by the Mars rover Opportunity. *Science* 324(5930):1058–1061, 2009.

[3] Derek Seward, Frank Margrave, Ian Sommerville, and Richard Morrey. LUCIE the robot excavator-design for system safety. *Robotics and Automation, 1996. Proceedings., 1996 IEEE International Conference on* 1:963–968, 1996.

[4] Defense Advanced Research Projects Agency (DARPA), DARPA Robotics Challenge (DRC) and Virtual Robotics Challenge (VRC). 2015. [Online]. Available: http://theroboticschallenge.org/about

[5] Sangok Seok, Aiping Wang, Meng Yee Chuah, David Otten, Jiandong Lang, and Sangbae Kim. Design principles for highly efficient quadrupeds and implementation on the MIT Cheetah robot. *Robotics and Automation (ICRA), 2013 IEEE International Conference on*, 3307–3312, 2013.

[6] Cornell Weifhr, Aaron Johnson, Aaron Peck, Zachary McCord, Allison Naaktgeboren, Philip Gianfortoni, Maneul Gonzalez-Rivero, Ross Hatton and Howie Choset. Design of a modular snake robot. *Intelligent Robots and Systems, 2007. IROS 2007. IEEE/RSJ International Conference on*, 2609–2614, 2007.

[7] Gregory Dudek, Philippe Giguere, Jim Zacher, Evangelos Milios, Hui Liu, Pifu Zhang, Marti Buehler, Christina Georgiades, Chris Prahacs, Shane Saunderson and others. Aqua: An amphibious autonomous robot. *Computer*. (1): 46–53, 2007.

[8] Samir Bouabdallah, Pierpaolo Murrieri and Rolan Siegwart. Design and control of an indoor micro quadrotor. *Robotics and Automation, 2004. Proceedings. ICRA'04. 2004 IEEE International Conference on*, 54393–4398, 2004.

[9] Boston Dynamics. Atlas - the agile anthropomorphic robot. 2013. [Online] Available: $http://www.bostondynamics.com/robot_Atlas.html$

[10] Ichiro Kato, Sadamu Ohteru, Hiroshi Kobayashi, Katsuhiko Shirai, and Akihiko Uchiyama. Information-power machine with senses and limbs. *On Theory and Practice of Robots and Manipulators*, 11–24, 1974.

[11] Bruno Andreotti, Yoël Forterre, and Olivier Pouliquen. Granular media: between fluid and solid. 2013.

[12] Jeffrey Aguilar, Tingnan Zhang, Feifei Qian, Mark Kingsbury, Bengamin McInroe, Nicole Mazouchova, Chen Li, Ryan Maladen, Chaohui Gong, Matt Travers, Ross L. Hatton, Howie Choset, Paul B. Umbanhowar and Daniel I. Goldman. A review on locomotion robophysics: the study of movement at the intersection of robotics, soft matter and dynamical systems, in review. *Reports on Progress in Physics*, 2015.

[13] Chen Li, Tingnan Zhang and Daniel I. Goldman. A terradynamics of legged locomotion on granular media. *Science*, 339(6126):1408–1412, 2013.

[14] Ill-Woo Park, Jung-Yup Kim, Jungho Lee, and Jun-Ho Oh. Mechanical design of humanoid robot platform KHR-3 (KAIST humanoid robot 3: HUBO. *Humanoid Robots, 2005 5th IEEE-RAS International Conference on*, 321–326, 2005.

[15] Jeffrey Aguilar, Alex Lesov, Kurt Wiesenfeld and Daniel I Goldman. Lift-off dynamics in a simple jumping robot. *Physical review letters*, 109(17):174301, 2012.

[16] Jeffrey Aguilar and Daniel I. Goldman. Robophysical study of jumping dynamics on granular media. *Nature Physics*, 2015.

[17] Ryan D Maladen, Yang Ding, Paul B Umbanhowar and Daniel I Goldman. Undulatory swimming in sand: experimental and simulation studies of a robotic sandfish. *The International Journal of Robotics Research*, 30(7):793–805, 2011.

[18] Daniel I Goldman, Haldun Kmsuoglu and Daniel E Koditschek. March of the sandbots. 2009.

[19] Feifei Qian and Daniel I Goldman. The dynamics of legged locomotion in heterogeneous terrain: universality in scattering and sensitivity to initial conditions. *RSS*, 2015.

[20] Ryan D Maladen, Yang Ding, Paul B Umbanhowar, Adam Kamor and Daniel I Goldman. Mechanical models of sandfish locomotion reveal principles of high performance subsurface sand-swimming. *Journal of The Royal Society Interface*, 8(62):1332–1345, 2011.

[21] J Shäfer, S Dippel and DE Wolf. Force schemes in simulations of granular materials. *Journel de physique I*, 6(1):5–20, 1996.

[22] Heinrich M Jaeger, Sidney R Nagel and Robert P Behringer. Granular solids, liquids, and gases. *Reviews of Modern Physics*, 68(4):1259, 1996.

[23] Trushant S Majmudar and Robert P Behringer. Contact force measurements and stress-induced anisotropy in granular materials. *Nature*, 435(7045):1079–1082, 2005.

[24] R Albert, MA Pfeifer, A-L Barabasi and P Schiffer. Slow drag in a granular medium. Physical review letters, 82(1):205, 1999.

[25] CR Wassgren, JA Cordova, R Zenit and A Karion. Dilute granular flow around an immersed cylinder. *Physics of Fluids (1994-present)*, 15(11):3318-3330, 2003.

[26] Daniel I Goldman and Paul Umbandhowar. Scaling and dynamics of sphere and disk impact into granular media. *Physical Review E*, 77(2):021308, 2008.

[27] Pierre Jop, Yoël Forterre, Olivier Pouliquen. A constitutive law for dense granular flows. *Nature*, 441(7094):727–730, 2006.

[28] Ronald Midgley Nedderman. Statics and kinematics of granular materials. 2005.

[29] JL Finney. Random packings and the structure of simple liquids. I. The geometry of random close packing. *Proceedings of the Royal Society of London A: Mathematical, Physical and Engineering Sciences*, 319(1539):479–493, 1970.

[30] Melissa Jerkins, Matthias Schröter, Harry L Swinney, Tim J Senden, Mohammad Saadatfar and Tomaso Aste. Onset of mechanical stability in random packings of frictional spheres. *Physical review letters*, 101(1):018301, 2008.

[31] Andrew Schofield and Peter Wroth. Critical state soil mechanics. 1968.

[32] Chen Li, Paul B Umbanhowar, Haldun Komsuoglu, Daniel E Koditschek and Daniel I Goldman. Sensitive dependence of the motion of a legged robot on granular media. *Proceedings of the National Academy of Sciences*, 106(9):3029–3034, 2009.

[33] SC Tsinontides and R Jackson. The mechanics of gas fluidized beds with an interval of stable fluidization. *Journal of Fluid Mechanics*, 255237–274, 1993.

[34] Nicole Mazouchova, Paul B Umbanhowar and Daniel I Goldman. Flipper-driven terrestial locomotion of a sea turtle-inspired robot. *Bioinspiration & Biomimetics*, 8(2):026007, 2013.

[35] Chen Li, Aaron M Hoover, Paul Birkmeyer, Paul B Umbanhowar, Ronald S Fearing and Daniel I Goldman. Systematic study of the performance of small

robots on controlled labratory substrates. *SPIE Defense, Security, and Sensing*, 76790Z–76790Z, 2010.

[36] Feifei Qian, Tignan Zhang, Wyatt Korff, Paul B Umbanhowar, Robert J Full and Daniel I Goldman. Principles of appendage design in robots and animals determining terradynamic performance on flowable ground. *Bioinspiration & biomimetics*, 10(5):056014, 2015.

[37] Martijn Wisse, Arend L Schwab, and RQ vd Linde. A 3D passive dynamic biped with yaw and roll compensation. *Robotica*, 19(03):275–284, 2001.

[38] Karl E. Zelik, Tzu-Wei P. Huan, Peter G. Adamczyk and Arthur D. Kuo. The role of series ankle elasticity in bipedal walking. *Journal of theoretical biology*, 346:75–85, 2014.

[39] Aaron D. Ames. Human-inspired control of bipedal walking robots. *Automatic Control, IEEE Transactions on*, 59(5):1115-1130, 2014.

[40] Alireza Ramezani, Jonathan W Hurst, Kaveh Akbari Hamed, and J.W. Grizzle. Performance analysis and feedback control of ATRIAS, a three-dimensional bipedal robot. *Journal of Dynamic Systems, Measurement, and Control*, 136(2): 021012, 2014.

[41] Kazi Rushdi, Derek Koop and Christine Q. Wu. Experimental studies on passive dynamic bipedal walking. *Robotics and Autonomous Systems*, 62(4):446–455, 2014.

[42] Juan Fang and Kenneth J Hunt. Foot trajectory approximation using the pendulum model of walking. *Medical & Biological Engineering & Computing*, 52(1): 45–52, 2014.

[43] Jin-Ichi Yamaguchi, Atsuo Takanishi and Ichiro Kato Development of a biped walking robot adapting to a horizontally uneven surface. *Intelligent Robots and Systems' 94.'Advanced Robotic Systems and the Real World', IROS'94. Proceedings of the IEEE/RSJ/GI International Conference on*, 21156-1163, 1994.

[44] Scott Kuindersma, Robin Deits, Maurice Fallo, Andrés Valenzuela, Hongkai Dai, Frank Permeneter, Twan Koolen, Pat Marion and Russ Tedrake. Optimization-based locomotion planning, estimation, and control design for the atlas humanoid robot. *Autonomous Robots*, 1–27, 2015.

[45] Steve Collins, Andy Ruina, Russ Tedrake and Martijn Wisse. Efficient bipedal robots based on passive-dynamic walkers. *Science*, 307(5712):1082–1085, 2005.

[46] Joel Chestnutt, Manfred Lau, German Cheung, James Kuffner, Jessica Hodgins, and Takeo Kanade. Footstep planning for the honda asimo humanoid. *Robotics and Automation, 2005. ICRA 2005. Proceedings of the 2005 IEEE International Conference on*, 629–634, 2005.

[47] J-H Kim, H-S Shim, H-S Kim, M-J Jung, LH Choi, and J-O Kim. A cooperative multi-agent system and its real time application to robot soccer. *Robotics and Automation, 1997. Proceedings., 1997 IEEE International Conference on*, 1:638–643, 1997.

[48] Pierre-Brice Wieber. Trajectory free linear model predictive control for stable walking in the presence of strong perturbations. *Humanoid Robots, 2006 6th IEEE-RAS International Conference on*, 137–142, 2006.

[49] Jung-Yup Kim, Ill-Woo Park and Jun-Ho Oh. Walking control algorithm of biped humanoid robot on uneven and inclined floor. Journal of Intelligent and Robotic Systems, 48(4):457–484, 2007.

[50] Shuuji Kajita, Fumio Kanehiro, Kenji Kaneko, Kazuhito Yokoi, and Hirohisa Hirukawa. The 3D Linear Inverted Pendulum Mode: A simple modeling for a biped walking pattern generation. *Intelligent Robots and Systems, 2001. Proceedings. 2001 IEEE/RSJ International Conference on*, 1:239–246, 2001.

[51] Michael J MacLellan and Aftab E Patla. Adaptations of walking pattern on a compliant surface to regulate dynamic stability. *Experimental brain research*, 173 (3):521–530, 2006.

[52] Shunsuke Komizunai, Atsushi Konno, Satoko Abiko, and Masaru Uchiyama. Development of a static sinkage model for a biped robot on loose soil. *System Integration (SII), 2010 IEEE/SICE International Symposium on*, 61–66, 2010.

[53] Steven H Collins, Martijn Wisse and Andy Ruina. A three-dimensional passive-dynamic walking robot with two legs and knees. *The International Journal of Robotics Research*, 20(7):607-615, 2001.

[54] Jonathan Hurst, Jessy W. Grizzle. MARLO robot. 2012. [Online] Available: *http : //web.eecs.umich.edu/ grizzle/papers/robotics.html*

[55] Yildirim Hurmuzlu, Frank Génot, and Bernard Brogliato. Modeling, stability and control of biped robots: a general framework. *Automatica*, 40(10):1647–1664, 2004.

[56] Bart Koopman, Henk J Grootenboer, and Henk J de Jongh. An inverse dynamics model for the analysis, reconstruction and prediction of bipedal walking. *Journal of Biomechanics*, 28(11):1369–1376, 1995.

[57] Arthur D. Kuo. Stabilization of lateral motion in passive dynamic walking. *The International journal of robotics research*, 18(9):917–930, 1999.

[58] Chrisine Chevallereau, Jessy W. Grizzle and Ching-Long Shih. *Robotics, IEEE Transactions on*, 25(1):37–50, 2009.

[59] Jo Yung Wong and others. Terramechanics and off-road vehicles. 1989.

[60] James Lighthill. Mathematica Biofluiddynamics. *Society for Industrial & Applied Mathematics, US*, 1975.

[61] RE Johnson and CJ Brokaw. Flagellar hydrodynamics. A comparison between resistive-force theory and slender-body theory. *Biophysical journal*, 25(1):113, 1979.

[62] Bruce Rodenborn, Chih-Hung Chen, Harry L Swinney, Bin Liu, and HP Zhang. Propulsion of microorganisms by a helical flagellum. *Proceedings of the National Academy of Sciences*, 110(5):E338-E347, 2013.

[63] Hesam Askari and Ken Kamrin. Intrusion in heterogeneous materials: Simple global rules from complex micro-mechanics. *arXiv preprint arXiv:1510.02966*, 2015.

[64] Thierry M Lejeune, Patrick A Willems and Norman C Heglund. Mechanics and energetics of human locomotion on sand. *The Journal of Experimental Biology*, 201(13):2071–2080, 1998.

[65] Nick Gravish, Paul B Umbanhowar, and Daniel I Goldman. Force and flow transition in plowed granular media. *Physical review letters*, 105(12):128301, 2010.

[66] Stephen M Gatesy. Guineafowl hind limb function. I: Cineradiographic analysis and speed effects. *Journal of Morphology*, 240(2):115–125, 1999.

[67] A. Tasora. Chrono Engine, an open source physics–based dynamics simulation engine. 2006.

[68] Yang Ding, Nick Gravish, and Daniel I Goldman. Drag induced lift in granular media. *Physical review letters*, 106(2):028001, 2011.

[69] Pranav A Bhounsule, Jason Cortell, Anoop Grewal, Bram Hendriksen, JG Daniël Karssen, Chandana Paul and Andy Ruina. Low-bandwidth reflex-based control for lower power walking: 65 km on a single battery charge. *The International Journal of Robotics Research*, 33(10):1305–1321, 2014.

[70] Chrisitan Hubicki, Jesse Grimes, Mikhail Jones, Daniel Renjewski, Alexander Spröwitz, Andy Abate and Jonathan Hurst. ATRIAS: Enabling agile biped locomotion with a template-driven approach to robot design. *Submitted to International Journal of Robotics Research*, 2014.

[71] Shuuji Kajita, Fumio Kanehiro, Kenji Kaneko, Kiyoshi Fujiwara, Kensuke Harada, Kazuhito Yokoi, and Hirohisa Hirukawa. Biped walking pattern generation by using preview control of zero-moment point. *Robotics and Automation, 2003. Proceedings. ICRA'03. IEEE International Conference on*, 2:, 1620–1626, 2003.

[72] Christian M Hubicki and Jonathan W Hurst. Running on soft ground: Simple, energy-optimal disturbance rejection. *International Conference on Climbing and Walking Robots (CLAWAR)*, 2012.

[73] Kelly M Dorgan, Sanjay R Arwade and Peter A Jumars. Worms as wedges: Effects of sediment mechanics on burrowing behavior. *Journal of Marine Research*, 66(2):219–254, 2008.

[74] Kelly M Dorgan, Peter A Jumars, Bruce Johnson, BP Boudreau and Eric Landis. Burrowing mechanics: burrow extension by crack propagation. *Nature*, 433 (7025):475–475, 2005.